DOI: 10.1002/ejic.200900558

Photoluminescent Porous Modular Lanthanide–Vanadium–Organic Frameworks

João Rocha,*[a] Filipe A. Almeida Paz,*[a] Fa-Nian Shi,[a] Rute A. S. Ferreira,[b] Tito Trindade,[a] and Luís D. Carlos[b]

Keywords: Metal–organic frameworks / Secondary building units / Self-assembly / Luminescence

Modular mixed metal-organic frameworks with lanthanide centres $M_4[M_{12}V_{24}O_{24}(OH)_8(H_2hedp)_8(Hhedp)_{16}(H_2O)_{64+n}]\cdot 88+y(H_2O)$ (M^{3+} = Y^{3+}, Ce^{3+}, Sm^{3+}, Eu^{3+}, Tb^{3+}, Gd^{3+}, Er^{3+}; H_5hedp = etidronic acid), have been reported. The compounds have been prepared by (i) slow evaporation of the solvent to afford large single-crystals of the Y^{3+}, Ce^{3+} and Er^{3+}compounds and (ii) facile one-pot synthesis (at ambient conditions) overnight to yield microcrystalline Y^{3+}, Ce^{3+}, Sm^{3+}, Eu^{3+}, Tb^{3+} and Gd^{3+} solids. Framework construction has been shown to be modular and based on the self-assembly of cyclic trinuclear $[V_3O_3(OH)(H_2hedp)(Hhedp)_2]^{6-}$ anionic units with cationic $\{MO_8\}$ or $\{MO_9\}$ aqua-based lanthanide complexes (with dodecahedral, square antiprismatic or tricapped trigonal prismatic coordination geometries), which gives rise to unprecedented trinodal networks (having 2- and 4-connected nodes) with a total Schäfli symbol of $\{4.8^3.10^2\}_2\{4^2.8^4\}\{8\}_2$. The anionic charge of the networks is balanced by highly disordered trivalent lanthanide cations in the channels. The compounds have been studied by single-crystal and powder X-ray diffraction, vibrational spectroscopy (FTIR), thermogravimetry, optical and scanning electron microscopy and elemental analysis. The photoluminescence properties of selected compounds have been investigated. Intriguingly, the co-existence of V^{4+} and Eu^{3+} cations in the same material allows the fine tuning of the photoluminescence emission from white to purplish-blue, by changing the excitation wavelength.

Introduction

Crystalline coordination-based, multi-dimensional compounds, known as coordination polymers or metal–organic frameworks, MOFs, are amid the most investigated materials in the last decade.[1] The seemingly endless combination of various metal centres with multipodal organic ligands results in the formation of fascinating architectures, which may lead to applications of industrial interest. Examples of the applications of functional MOFs encompass sensors (for solvents,[2] pH or gases[3]), gas storage,[4] batteries[5] and magnetic[6] and photoluminescent[7] materials. The design of MOF structures is currently based on typical bottom-up synthetic approaches that use the concept of rigid building blocks (secondary building units – SBUs). This strategy has been successfully employed for inorganic frameworks,[8] and among MOFs, the most striking examples of structure solution that uses the SBU concept are those of the MIL-100 and MIL-101 materials.[9] We have been interested in the design and preparation of novel MOF materials[10] assembled from lanthanide cations[11–14] and organic ligands containing carboxylate[11] or phosphonate[12,13] binding groups. The latter mimic the tetrahedral geometry of the building units of zeolites and may also direct the formation of highly robust frameworks.

Etidronic acid, H_5hedp, is a flexible bisphosphonic acid molecule, which has been largely self-assembled with both transition metals[15] and lanthanides.[13,16–18] Our work with this ligand encompasses 2D/3D systems exhibiting, for the first time, single-crystal-to-single-crystal crystal conversion,[13] chain-type photoluminescent materials templated by 1,4-diaminobutane[16] and the formation of hexameric $[Ge_6(\mu_2\text{-}OH)_6(C_2H_4O_7P_2)_6]^{6-}$ moieties that close pack with aromatic ambidentate molecules to form supramolecular organic–inorganic crystalline hybrids.[19]

Whilst searching the literature, an unusual cyclic trinuclear anionic unit, described by Aleksandrov and coworkers, came to our notice, which is composed of H_{5-x}-hedp^{-x} residues and V^{4+} centres.[20] This unit, which has much potential for the crystal engineering of multi-dimensional MOF structures, has not been previously used for this purpose. Indeed, it (i) is a highly negatively-charged "brick", which requires the presence of several cations to balance the crystal charge, (ii) contains several *exo*-oxygen atoms (from six phosphonate groups) available for coordi-

[a] Department of Chemistry, CICECO, University of Aveiro, 3810-193 Aveiro, Portugal
Fax: +351-234-401470
E-mail: rocha@ua.pt
filipe.paz@ua.pt
[b] Department of Physics, CICECO, University of Aveiro, 3810-193 Aveiro, Portugal

Supporting information for this article is available on the WWW under http://dx.doi.org/10.1002/ejic.200900558.

nating a large number of metal centres, and (iii) is a unit with a large volume and triangular geometry that may prevent effective close packing in the solid and, thus, may direct the self-assembly of frameworks with large empty voids. Zheng and co-workers recently reported a similar approach for the use of dimeric $[Ru_2(Hhedp)_2(H_2O)_2]^{3-}$ anionic units to produce layered and 3D lanthanide–organic frameworks with PtS topology.[17]

Here, we wish to report the use of the cyclic trinuclear anionic unit of Aleksandrov et al. as an effective and robust SBU for the construction of a series of 3D modular trinodal (with 2- and 4-connected nodes) mixed-metal–organic frameworks, $M_4[M_{12}V_{24}O_{24}(OH)_8(H_2hedp)_8(Hhedp)_{16}(H_2O)_{64+n}]\cdot 88+y(H_2O)$ (where M^{3+} = Y^{3+}, Ce^{3+}, Sm^{3+}, Eu^{3+}, Tb^{3+}, Gd^{3+} and Er^{3+}). This SBU unit may be prepared at room temperature and it self-assembles with lanthanide centres to afford microcrystalline powders in excellent yields. The simultaneous presence in these MOFs of a transition metal (V^{4+}) and a trivalent lanthanide ion (Eu^{3+}) leads to compounds that are multi-wavelength emitters, whose emission colour is easily tuned from white to purplish-blue by simply changing the excitation wavelength.

Results and Discussion

General Considerations of the Synthesis

The series of modular mixed-metal–organic framework materials, generally formulated as $M_4[M_{12}V_{24}O_{24}(OH)_8(H_2hedp)_8(Hhedp)_{16}(H_2O)_{64+n}]\cdot 88+y(H_2O)$ (M^{3+} = Y^{3+}, Ce^{3+}, Sm^{3+}, Eu^{3+}, Tb^{3+}, Gd^{3+} and Er^{3+}; H_5hedp = etidronic acid), have been prepared by two routes: (i) by slow evaporation of the water of the autoclave mother liquors (see Experimental Sections), which affords large and well-formed Y^{3+} (**1s**), Ce^{3+} (**2s**) and Er^{3+} (**6s**) single-crystals (Figures S1–S3 in the Supporting Information); (ii) by facile one-pot synthesis of Y^{3+} (**1**), Ce^{3+} (**2**), Sm^{3+} (**3**), Eu^{3+} (**4**), Tb^{3+} (**5**) and Gd^{3+} (**7**) materials, at ambient temperature, by adding all reactants together and by magnetic stirring overnight (see Experimental Section).

Although the materials prepared by route (ii) are poorly crystalline, phase-purity could be confirmed by several characterization techniques, in particular powder X-ray diffraction (from whole powder-diffraction-pattern profile fittings by using Le Bail extraction, Figures S4–S8 in the Supporting Information).

It is thus reasonable to conclude that the self-assembly of the framework occurs in the same way independently of the synthetic approach adopted. On the basis of this, we rationalized the construction of the materials in terms of a typical modular fashion, which is described in detail in the following sections.

The Anionic $[V_3O_3(OH)(H_2hedp)(Hhedp)_2]^{6-}$ Building Block

The presence of etidronic acid (H_5hedp) and $VOSO_4$ in aqueous solution immediately leads to the formation of the cyclic trinuclear anionic unit $[V_3O_3(OH)(H_2hedp)(Hhedp)_2]^{6-}$, which contains three V^{4+} metallic centres at the corners of a triangle and which is bridged through three etinodrate residues. These etinodrate residues coordinate via deprotonated phosphonate groups with typical *syn*,*syn*-bridging coordination modes to ultimately form six-membered chelate rings with each metal ion (Figure 1). This rigid anionic unit has been reported by Aleksandrov and collaborators[20] for a crystalline ($P6_3/m$) structure with charge-balancing diethylammonium cations. The asymmetric unit perfectly accommodates one fully-occupied V^{4+} metal centre and a single etinodrate residue, $H_{5-x}hedp^{-x}$. However, in the tetragonal $M_4[M_{12}V_{24}O_{24}(OH)_8(H_2hedp)_8(Hhedp)_{16}(H_2O)_{64+n}]\cdot 88+y(H_2O)$ [M^{3+} = Y^{3+} (**1s**), Ce^{3+} (**2s**) and Er^{3+} (**6s**)] frameworks herein reported, this anionic unit is generated by mirror symmetry, which requires the presence of two crystallographically independent V^{4+} centres and another two $H_{5-x}hedp^{-x}$ ligands and that one of each is only half occupied in the asymmetric unit (Figure 1). It is important to note that even though $H_{5-x}hedp^{-x}$ does not show mirror symmetry in the plane containing the two phosphorus atoms, the coordination to the V^{4+} centres is not affected if the ligand is "flipped" by 180°. This leads to statistical disorder associated with the methyl and hy-

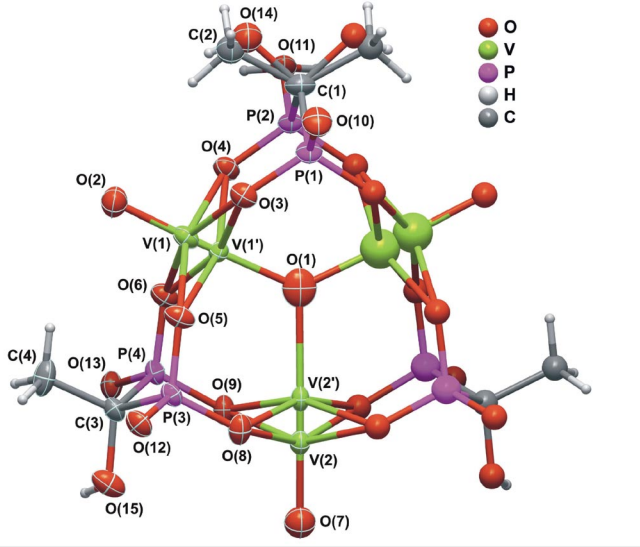

	1s (Y^{3+})	2s (Ce^{3+})	6s (Er^{3+})
V(1) / V(1')	63.5(2)% / 36.5(2)%	68.2(9)% / 31.8(9)%	58.8(1)% / 41.2(1)%
V(2) / V(2')	70.2(1)% / 29.7(1)%	64.4(1)% / 35.6(1)%	83.3(7)% / 16.7(7)%

Figure 1. Schematic representation of the cyclic trinuclear anionic unit $[V_3O_3(OH)(H_2hedp)(Hhedp)_2]^{6-}$, emphasizing the disorder and rates of occupancy of the V^{4+} centres for the three single-crystal X-ray determinations. Atoms in the asymmetric unit are represented by thermal ellipsoids drawn at the 50% probability level, except for C(2) and O(14) (methyl and hydroxido disordered groups), which are represented by isotropic spheres of thermal motion (anionic unit taken from the structure of compound **6s**). All remaining non-hydrogen atoms are represented in ball-and-stick mode (symmetry transformation used to generate the entire trinuclear anionic unit: x, y, $2 - z$). Hydrogen atoms have been omitted for clarity. For selected bond lengths (in Å) and angles (in °) see Tables 1 and 2, respectively.

droxido groups, a feature that was modelled for this H_{5-x}-hedp^{-x} residue (see Experimental Section), and ultimately creates a *pseudo*-mirror symmetry for this chelating ligand.

Although the cyclic trinuclear unit is generated by different symmetry operations in our crystal structures and in that of Aleksandrov et al.,[20] we also observed positional structural disorder for the V^{4+} centres: the distances between the disordered centres are almost identical; V(1)···V(1′) and V(2)···V(2′) range from 0.710(2) to 0.784(5) Å and 0.788(5) to 0.895(9) Å, respectively. These values are, in general, significantly different from that reported for the stand-alone complex [0.908(6) Å].[20] This disorder was modelled with refineable rates of occupancy, which converged to the values shown in Figure 1. It is interesting to note that in the crystal structure of the stand-alone trinuclear anionic complex, the structural disorder was also extended into the bridging H_{5-x}hedp^{-x} anionic ligands (in particular the oxygen atoms of the phosphonate groups). This structural feature is completely absent in the single-crystal determinations of **1s**, **2s** and **6s**, most likely because of the low temperature used for data collection (150 K vs. 298 K used by Aleksandrov et al.). The coordination geometry of all crystallographically independent V^{4+} centres (among the three single-crystal X-ray determinations) may be seen to be very similar and as highly distorted octahedra [overall ranges for the polyhedral angles: for V(1), 76.3(2)–104.2(3)° and 153.2(3)–178.2(2)°; for V(1′), 79.3(3)–102.7(4)° and 156.8(4)–179.6(1)°; for V(2), 76.7(1)–105.0(2)° and 152.1(4)–178.8(1)°; for V(2′), 77.1(1)–103.4(4) and 156.1(8)–177.8(6)°; see Table 2 for more details]. For the most probable coordination environments [V(1) and V(2)], this coordination geometry may be further envisaged as those classified by Boudin et al.[21] as 1+4+1, with one short (V=O), four intermediate (V–O) and one long (V–O, *trans* to V=O) bonds (Tables 1 and 2; Figure 1).

The nature of disorder of each V^{4+} metal centre leads to the peculiarity that the oxido groups of V(1) or V(2) [O(2) or O(7), respectively] are in fact a coordinated hydroxido ligand in the coordination sphere of the less-probable V(1′) and V(2′) centres (note the long V–O distances found in the 2.282(8)–2.489(4) Å range, Table 1). In a similar fashion, the central bridging μ_3-O(1) atom becomes the oxido ligand in the V(1′) or V(2′) coordination spheres. For the two most probable positions of the V^{4+} centres [V(1) and V(2)], the *trans* influence of the oxido group is markedly present, with the short V=O bonds [ranging from 1.533(11) and 1.571(7) Å]. This effect strongly shifts the metal centres [average values of ca. 0.40 and 0.46 Å] from the equatorial plane formed by the intermediate V–O bonds [for V(1), 1.975(4)–2.022(6) Å; for V(2), 1.981(4)–2.014(6) Å]. This leaves the μ_3-O(1) atom at unusually large average distances of 2.54 and 2.90 Å [for V(1) and V(2), respectively; Figure 1 and Table 1].

For V(1′) and V(2′), the *trans* influence is not so markedly present; the metal centres are only shifted by ca. 0.35 and 0.39 Å, respectively, from the equatorial plane. In fact, while the V–O bond ranges for the equatorial oxygen atoms remain essentially unchanged [1.946(6)–2.016(7) Å and 1.941(6)–1.996(7) Å], the distances for those expected as being V=O are considerably longer [average values of ca. 1.79 and 2.05 Å].

Overall, it is possible to distinguish two markedly distinct conformations for the cyclic trinuclear complex: one with all V^{4+} centres occupying the "outer" positions (higher

Table 1. Selected bond lengths (in Å) for $M_4[M_{12}V_{24}O_{24}(OH)_8(H_2hedp)_8(Hhedp)_{16}(H_2O)_{64+n}]\cdot 88+y(H_2O)$ [where M^{3+} = Y^{3+} (**1s**), Ce^{3+} (**2s**) and Er^{3+} (**6s**)] (n = 8 for **2s**).

	1s (Y^{3+})	**2s** (Ce^{3+})	**6s** (Er^{3+})		**1s** (Y^{3+})	**2s** (Ce^{3+})	**6s** (Er^{3+})
M(1)–O(13)	2.274(5)	2.388(5)	2.260(4)	M(2)–O(12)	2.251(5)	2.405(5)	2.241(4)
M(1)–O(1W)	2.439(6)	2.563(5)	2.416(4)	M(2)–O(2W)	2.408(7)	2.574(7)	2.374(5)
				M(2)–O(3W)	2.426(6)	2.542(6)	2.412(5)
				M(2)–O(4W)	2.347(7)	2.565(6)	2.337(5)
				M(2)–O(5W)	–	2.694(12)	–
V(1)–O(1)	2.532(6)	2.634(6)	2.456(6)	V(1′)–O(1)	1.782(13)	1.852(10)	1.745(7)
V(1)–O(2)	1.565(11)	1.564(7)	1.571(7)	V(1′)–O(2)	2.313(4)	2.347(4)	2.282(8)
V(1)–O(3)	1.997(6)	1.983(5)	2.001(4)	V(1′)–O(3)	1.970(6)	1.946(6)	1.971(4)
V(1)–O(4)	2.022(6)	2.011(5)	2.018(4)	V(1′)–O(4)	1.998(6)	1.983(6)	2.003(4)
V(1)–O(5)	1.990(6)	1.979(5)	1.975(4)	V(1′)–O(5)	2.016(7)	2.015(6)	1.993(4)
V(1)–O(6)	1.998(6)	1.991(5)	1.994(4)	V(1′)–O(6)	1.992(7)	1.975(6)	1.993(4)
V(2)–O(1)	2.949(1)	2.723(1)	3.039(1)	V(2′)–O(1)	2.055(17)	1.935(16)	2.173(14)
V(2)–O(7)	1.533(11)	1.555(11)	1.565(7)	V(2′)–O(7)	2.489(4)	2.343(1)	2.431(1)
V(2)–O(8)	2.014(6)	2.006(5)	1.987(4)	V(2′)–O(8)	1.981(7)	1.978(6)	1.941(6)
V(2)–O(9)	1.996(5)	1.993(5)	1.981(4)	V(2′)–O(9)	1.996(7)	1.991(5)	1.992(7)
P(1)–C(1)	1.823(11)	1.823(11)	1.814(8)	P(3)–C(3)	1.841(8)	1.838(7)	1.836(5)
P(1)–O(3)	1.533(5)	1.532(5)	1.527(4)	P(3)–O(5)	1.522(6)	1.528(5)	1.524(4)
P(1)–O(10)	1.497(8)	1.501(7)	1.496(6)	P(3)–O(8)	1.529(6)	1.536(5)	1.523(4)
P(2)–C(1)	1.825(11)	1.836(11)	1.818(9)	P(3)–O(12)	1.502(5)	1.501(5)	1.500(4)
P(2)–O(4)	1.532(5)	1.539(5)	1.532(4)	P(4)–C(3)	1.829(8)	1.839(7)	1.835(5)
P(2)–O(11)	1.513(8)	1.498(7)	1.505(6)	P(4)–O(6)	1.528(5)	1.532(5)	1.521(4)
				P(4)–O(9)	1.537(5)	1.532(5)	1.534(4)
				P(4)–O(13)	1.509(5)	1.507(5)	1.512(4)

Table 2. Selected bond angles (°) for the V^{4+} coordination environments present in $M_4[M_{12}V_{24}O_{24}(OH)_8(H_2hedp)_8(Hhedp)_{16}(H_2O)_{64+n}]\cdot 88+y(H_2O)$ [where $M^{3+} = Y^{3+}$ (**1s**), Ce^{3+} (**2s**) and Er^{3+} (**6s**)] ($n = 8$ for **2s**).[a]

	1s (Y^{3+})	**2s** (Ce^{3+})	**6s** (Er^{3+})		**1s** (Y^{3+})	**2s** (Ce^{3+})	**6s** (Er^{3+})
O(2)–V(1)–O(1)	178.2(2)	177.9(2)	177.9(2)	O(1)–V(1′)–O(2)	179.6(1)	178.3(3)	178.3(3)
O(2)–V(1)–O(3)	102.9(4)	104.2(3)	101.9(3)	O(1)–V(1′)–O(3)	99.1(5)	100.3(4)	98.4(3)
O(2)–V(1)–O(4)	99.6(4)	99.1(3)	99.5(3)	O(1)–V(1′)–O(4)	100.6(5)	102.7(4)	98.6(3)
O(2)–V(1)–O(5)	101.8(4)	103.0(3)	100.7(3)	O(1)–V(1′)–O(5)	101.1(5)	100.5(4)	102.1(3)
O(2)–V(1)–O(6)	101.3(4)	102.5(3)	101.1(3)	O(1)–V(1′)–O(6)	100.1(5)	98.6(4)	99.8(3)
O(3)–V(1)–O(1)	77.3(1)	76.9(2)	77.7(2)	O(3)–V(1′)–O(2)	81.1(3)	81.2(3)	81.6(2)
O(3)–V(1)–O(4)	88.8(2)	89.1(2)	88.58(17)	O(3)–V(1′)–O(4)	90.2(3)	91.0(3)	89.83(18)
O(3)–V(1)–O(6)	155.8(5)	153.2(3)	157.0(3)	O(3)–V(1′)–O(5)	84.6(3)	84.1(2)	85.44(18)
O(4)–V(1)–O(1)	78.6(1)	79.0(1)	78.4(2)	O(3)–V(1′)–O(6)	160.7(7)	160.9(5)	161.9(4)
O(5)–V(1)–O(1)	80.0(1)	78.9(1)	81.3(3)	O(4)–V(1′)–O(2)	79.1(3)	77.9(3)	79.8(2)
O(5)–V(1)–O(3)	84.6(2)	84.1(2)	85.11(17)	O(4)–V(1′)–O(5)	158.3(7)	156.8(4)	159.2(4)
O(5)–V(1)–O(4)	158.5(5)	157.9(3)	159.6(3)	O(5)–V(1′)–O(2)	79.3(3)	79.0(3)	79.5(2)
O(5)–V(1)–O(6)	91.2(2)	91.1(2)	91.30(17)	O(6)–V(1′)–O(2)	79.7(3)	79.8(3)	80.3(2)
O(6)–V(1)–O(1)	78.5(1)	76.3(2)	79.4(2)	O(6)–V(1′)–O(4)	87.4(3)	86.7(2)	87.41(18)
O(6)–V(1)–O(4)	86.6(2)	85.5(2)	86.98(17)	O(6)–V(1′)–O(5)	90.6(3)	90.5(3)	90.82(19)
O(7)–V(2)–O(1)	178.3(1)	178.8(1)	177.3(3)	O(1)–V(2′)–O(7)	177.0(1)	177.8(6)	175.5(5)
O(7)–V(2)–O(8)	104.6(3)	103.0(3)	105.0(2)	O(1)–V(2′)–O(8)	103.2(5)	101.1(4)	103.4(4)
O(7)–V(2)–O(9)	103.3(3)	102.0(3)	102.6(2)	O(1)–V(2′)–O(9)	100.6(5)	99.5(4)	99.6(4)
O(8)–V(2)–O(1)	76.7(1)	77.9(2)	76.9(1)	O(8)–V(2′)–O(7)	78.9(1)	80.4(1)	79.8(1)
$O(8)^{v}$–V(2)–O(8)	85.1(3)	86.8(3)	85.5(2)	$O(8)^{v}$–V(2′)–O(8)	86.9(4)	88.3(3)	88.1(4)
O(9)–V(2)–O(1)	75.4(1)	77.2(2)	75.5(1)	O(8)–V(2′)–O(9)	89.8(3)	90.0(2)	90.1(2)
O(9)–V(2)–O(8)	88.9(2)	89.2(2)	89.07(15)	O(8)–V(2′)–$O(9)^{v}$	156.1(8)	159.2(5)	156.8(7)
$O(9)$–V(2)–$O(8)^{v}$	152.1(4)	155.0(4)	152.3(2)	O(9)–V(2′)–O(7)	77.3(1)	79.0(1)	77.1(1)
$O(9)$–V(2)–$O(9)^{v}$	83.7(3)	84.1(3)	83.2(2)	O(9)–V(2′)–$O(9)^{v}$	83.7(4)	84.2(3)	82.6(3)

[a] Symmetry transformation used to generate equivalent atoms: (v) $x, y, 2 - z$.

probability of occurrence, Figure 2a), the other with the metal centres in the "inner" positions (lower probability of occurrence, Figure 2b). However, it is also possible to assume that other less-symmetrical conformations exist within the structure (Figure 2c, d) and that conformational change might occur simply as a result of thermal motion.

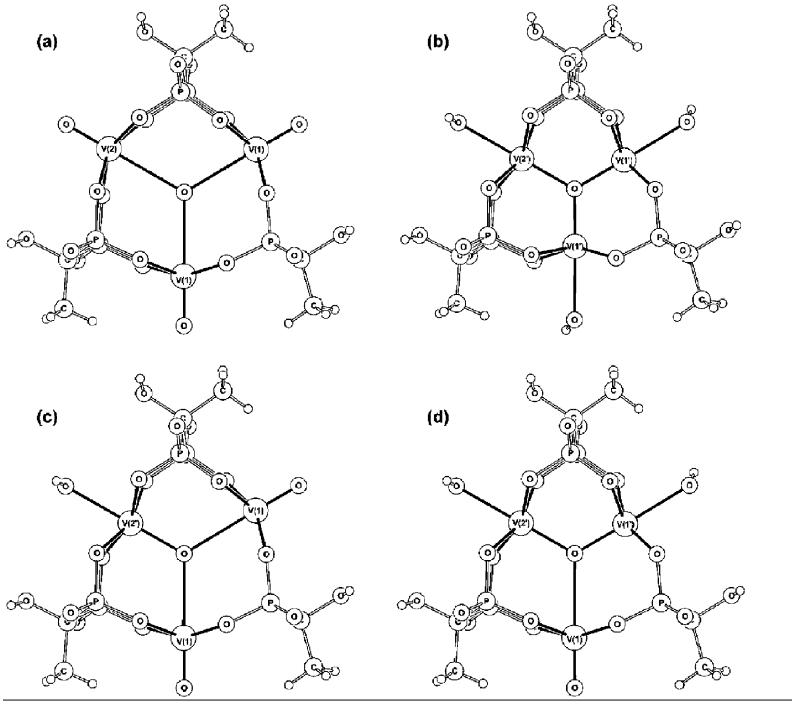

	1s (Y^{3+})	**2s** (Ce^{3+})	**6s** (Er^{3+})
V(1) / V(1')	63.5(2)% / 36.5(2)%	68.2(9)% / 31.8(9)%	58.8(1)% / 41.2(1)%
V(2) / V(2')	70.2(1)% / 29.7(1)%	64.4(1)% / 35.6(1)%	83.3(7)% / 16.7(7)%

Figure 2. Schematic representation of the four possible conformations for the cyclic trinuclear anionic unit $[V_3O_3(OH)(H_2hedp)(Hhedp)_2]^{6-}$. For clarity, only one position for the disordered $-C(CH_3)OH$ chemical moiety is represented.

Although this cannot be modelled by using the collected single-crystal X-ray diffraction data sets, it would account for the diffuse electron density found along the axis defined by each pair of disordered V^{4+} centres. Furthermore, for the less-probable conformation (Figure 2b), the distances between the V^{4+} centres are considerably smaller [average values: V(1′)···V(2′) 3.29 Å and V(1′)···V(1′)^{v} 3.17 Å; symmetry code: (v) *x*, *y*, –*z*] than those measured for the most-probable conformation [Figure 2a; average values: V(1)···V(1)^{v} 4.52 Å and V(1)···V(2) 4.65 Å]. Thus, the increased steric hindrance in the core of the cyclic trinuclear complex represented in Figure 2b may explain the unusually long V=O bonds (see above) and reinforce the possibility of the existence of the intermediate conformations described in Figure 2c,d, which lead to longer intermetallic distances [average values: V(1′)···V(2) 4.06 Å, V(1′)···V(1)^{v} 3.86 Å and V(2′)···V(1)^{v} 3.93 Å].

Lanthanide M(1) and M(2) SBUs: Coordination Environments

The most structurally relevant, crystallographically independent lanthanide centres are M(1) and M(2), which are directly coordinated to the $[V_3O_3(OH)(H_2hedp)(Hhedp)_2]^{6-}$ anionic units and establish physical connections and ultimately build up the frameworks. The charge-balancing lanthanide cations M(3)–M(5) do not seem to be directly involved in the self-assembly process. M(1) is coordinated to four-symmetry related O(13) atoms (from the anionic SBU units) and to four O(1W) water molecules, $\{MO_8\}$, with the overall coordination geometry of a slightly distorted dodecahedron: for the three crystal determinations, while the M(1)–O(1W) distances range from 2.416(4) to 2.563(5) Å, those for the M(1)–O(13) interaction are 2.260(4)–2.388(5) Å (Table 1). Interestingly, each bisphenoid of the dodecahedron contains two water molecules (located at the inner positions) and two O atoms from phosphonate groups (Figure 3) – these locations are a direct consequence of the formation of the spiral chains (see below). The O–M(1)–O

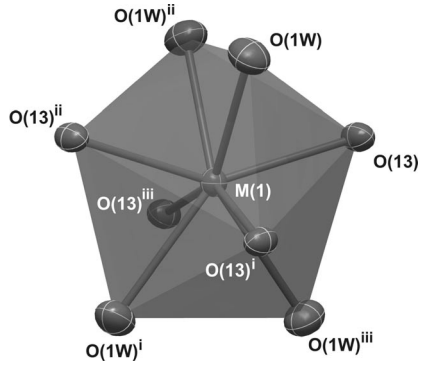

Figure 3. Schematic representation of the distorted dodecahedral $\{MO_8\}$ coordination environment of M(1) present in **1s**, **2s** and **6s**. Atoms are represented as thermal ellipsoids drawn at the 50% probability level. Symmetry transformations used to generate equivalent atoms: (i) *y*, 1 – *x*, 1.5 – *z*; (ii) 1 – *x*, 1 – *y*, *z*; (iii) 1 – *y*, *x*, 1.5 – *z*. For selected bond lengths (in Å) and angles (in °) see Tables 1 and 3, respectively.

Table 3. Selected bond angles (°) for the M(1) and M(2) coordination environments present in $M_4[M_{12}V_{24}O_{24}(OH)_8(H_2hedp)_8(Hhedp)_{16}(H_2O)_{64+n}]\cdot 88+y(H_2O)$ [where M^{3+} = Y^{3+} (**1s**), Ce^{3+} (**2s**) and Er^{3+} (**6s**)] (*n* = 8 for **2s**).[a]

	1s (Y^{3+})	**2s** (Ce^{3+})	**6s** (Er^{3+})		**1s** (Y^{3+})	**2s** (Ce^{3+})	**6s** (Er^{3+})
O(13)–M(1)–O(13)^{ii}	147.7(3)	147.0(2)	146.40(18)	O(12)–M(2)–O(12)^{iv}	115.8(3)	113.9(2)	117.5(2)
O(13)–M(1)–O(13)^{iii}	94.44(7)	94.62(6)	94.79(5)	O(12)–M(2)–O(2W)^{iv}	74.8(2)	72.9(2)	74.73(17)
O(13)–M(1)–O(1W)	77.6(2)	78.59(18)	76.64(14)	O(12)–M(2)–O(2W)	73.4(3)	68.9(2)	72.37(18)
O(13)–M(1)–O(1W)^{i}	141.9(2)	141.72(18)	143.09(14)	O(12)–M(2)–O(3W)	144.0(2)	141.45(19)	143.96(16)
O(13)–M(1)–O(1W)^{ii}	76.3(2)	74.61(18)	76.42(14)	O(12)–M(2)–O(3W)^{iv}	74.2(2)	71.62(18)	73.12(15)
O(13)–M(1)–O(1W)^{iii}	70.4(2)	71.22(18)	70.51(14)	O(12)–M(2)–O(4W)	81.1(3)	71.02(19)	81.4(2)
O(13)^{i}–M(1)–O(13)	94.44(7)	94.62(6)	94.79(5)	O(12)^{iv}–M(2)–O(4W)	139.4(2)	136.8(2)	138.34(18)
O(13)^{i}–M(1)–O(1W)	70.4(2)	71.22(18)	70.51(14)	O(12)–M(2)–O(5W)	–	123.03(12)	–
O(13)^{i}–M(1)–O(1W)^{i}	77.6(2)	78.59(18)	76.64(14)	O(12)^{iv}–M(2)–O(5W)	–	123.03(12)	–
O(13)^{i}–M(1)–O(1W)^{ii}	141.9(2)	141.72(18)	143.09(14)	O(12)–M(2)–O(4W)^{iv}	139.4(2)	136.8(2)	138.34(18)
O(13)^{i}–M(1)–O(1W)^{iii}	77.6(2)	74.61(18)	76.42(14)	O(2W)–M(2)–O(5W)	–	126.9(2)	–
O(13)^{i}–M(1)–O(13)^{ii}	94.44(7)	94.62(6)	94.79(5)	O(2W)^{iv}–M(2)–O(5W)	–	126.9(2)	–
O(13)^{i}–M(1)–O(13)^{iii}	147.7(3)	147.0(2)	146.40(18)	O(3W)–M(2)–O(2W)	140.1(3)	141.3(2)	140.72(18)
O(13)^{ii}–M(1)–O(1W)	76.3(2)	74.61(18)	76.42(14)	O(3W)^{iv}–M(2)–O(2W)^{iv}	140.1(3)	141.3(2)	140.72(18)
O(13)^{ii}–M(1)–O(1W)^{i}	70.4(2)	71.22(18)	70.51(14)	O(3W)–M(2)–O(2W)^{iv}	75.8(3)	74.6(3)	76.8(2)
O(13)^{ii}–M(1)–O(1W)^{ii}	77.6(2)	78.59(18)	76.64(14)	O(3W)–M(2)–O(3W)^{iv}	119.3(4)	129.3(3)	120.0(3)
O(13)^{ii}–M(1)–O(1W)^{iii}	141.9(2)	141.72(18)	143.09(14)	O(3W)–M(2)–O(4W)	72.3(3)	80.0(2)	71.7(2)
O(13)^{iii}–M(1)–O(1W)	141.9(2)	141.72(18)	143.09(14)	O(3W)–M(2)–O(4W)^{iv}	74.3(3)	81.7(2)	74.9(2)
O(13)^{iii}–M(1)–O(1W)^{ii}	70.4(2)	71.22(18)	70.51(14)	O(3W)–M(2)–O(5W)	–	64.65(15)	–
O(1W)–M(1)–O(1W)^{i}	131.1(2)	131.73(18)	130.52(14)	O(3W)^{iv}–M(2)–O(5W)	–	64.65(15)	–
O(1W)–M(1)–O(1W)^{iii}	131.1(2)	131.73(18)	130.52(14)	O(4W)–M(2)–O(2W)	144.9(3)	138.1(2)	145.83(19)
O(1W)^{i}–M(1)–O(1W)^{iii}	71.6(3)	70.7(3)	72.6(2)	O(4W)–M(2)–O(2W)^{iv}	76.7(4)	72.6(3)	78.5(3)
O(1W)^{ii}–M(1)–O(1W)	71.6(3)	70.7(3)	72.6(2)	O(4W)–M(2)–O(4W)^{iv}	110.6(6)	136.5(3)	109.8(5)
O(1W)^{ii}–M(1)–O(1W)^{i}	131.1(2)	131.73(18)	130.52(14)	O(4W)–M(2)–O(5W)	–	68.25(17)	–
O(1W)^{ii}–M(1)–O(1W)^{iii}	131.1(2)	131.73(18)	130.52(14)	O(4W)^{iv}–M(2)–O(5W)	–	68.25(17)	–

[a] Symmetry transformations used to generate equivalent atoms: (i) *y*, 1 – *x*, 1.5 – *z*; (ii) 1 – *x*, 1 – *y*, *z*; (iii) 1 – *y*, *x*, 1.5 – *z*; (iv) –1/2 + *y*, ½ + *x*, 1.5 – *z*.

bond angles along the bisphenoids range between 70.4(2) and 78.59(18)°, which clearly attests the small distortion degree of the polyhedra (Table 3).

M(2) has physical connections to two anionic SBUs and is thus composed of more water molecules and is more susceptible to a larger distortion degree of the coordination polyhedra. Indeed, in **2s**, because of the larger ionic radius of Ce^{3+}, Ce(2) is coordinated to an extra water molecule, $\{CeO_9\}$, relative to the analogous M(2) environment in **1s** and **6s**, $\{MO_8\}$ (Figure 4). In the latter two compounds, M(2) appears in a slightly distorted square-antiprism geometry, with one of the basal planes composed solely of water molecules [O(3W) and O(4W)] and the other of O(2W) and O(12) from phosphonate groups. Distortion of the square antiprism arises essentially from the varying M(2)–O distances observed for **1s** and **6s** because of the different chemical nature of the ligands (Table 1). Nevertheless, the internal O–M(2)–O angles are not very different: for example, by considering just the basal planes, the angles range from 71.7(2) to 78.5(3)° (Table 3). The inclusion of O(5W) in the coordination sphere of Ce(2) in **2s** leads to modifications of the coordination environment, which results in a distorted tricapped trigonal prism. This expansion of the coordination sphere seems to be only possible because of the larger ionic radius of Ce^{3+} (as emphasized above); the Ce(2)–O(5W) bond is significantly longer [2.694(12) Å] than the remaining analogous bonds (average value of 2.56 Å). The internal O–M(2)–O angles in compound **2s** range from 64.65(15)° [because of the proximity of O(5W) with the water molecules of the capped face – Figure 4] to 141.45(19)° (Table 3).

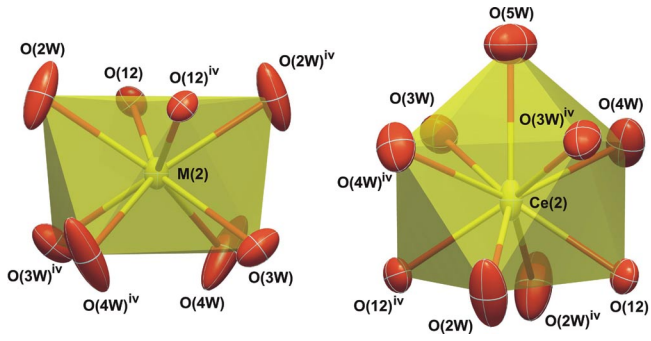

Figure 4. Polyhedral representations of the distorted (left) $\{MO_8\}$ square antiprismatic (**1s** and **6s**) and (right) $\{MO_9\}$ tricapped trigonal prismatic (**2s**) M(2) coordination environments. Atoms are represented as thermal ellipsoids drawn at the 50% probability level. Symmetry transformations used to generate equivalent atoms: (iv) –1/2 + *y*, ½ + *x*, 1.5 – *z*. For selected bond lengths (in Å) and angles (in °) see Tables 1 and 3, respectively.

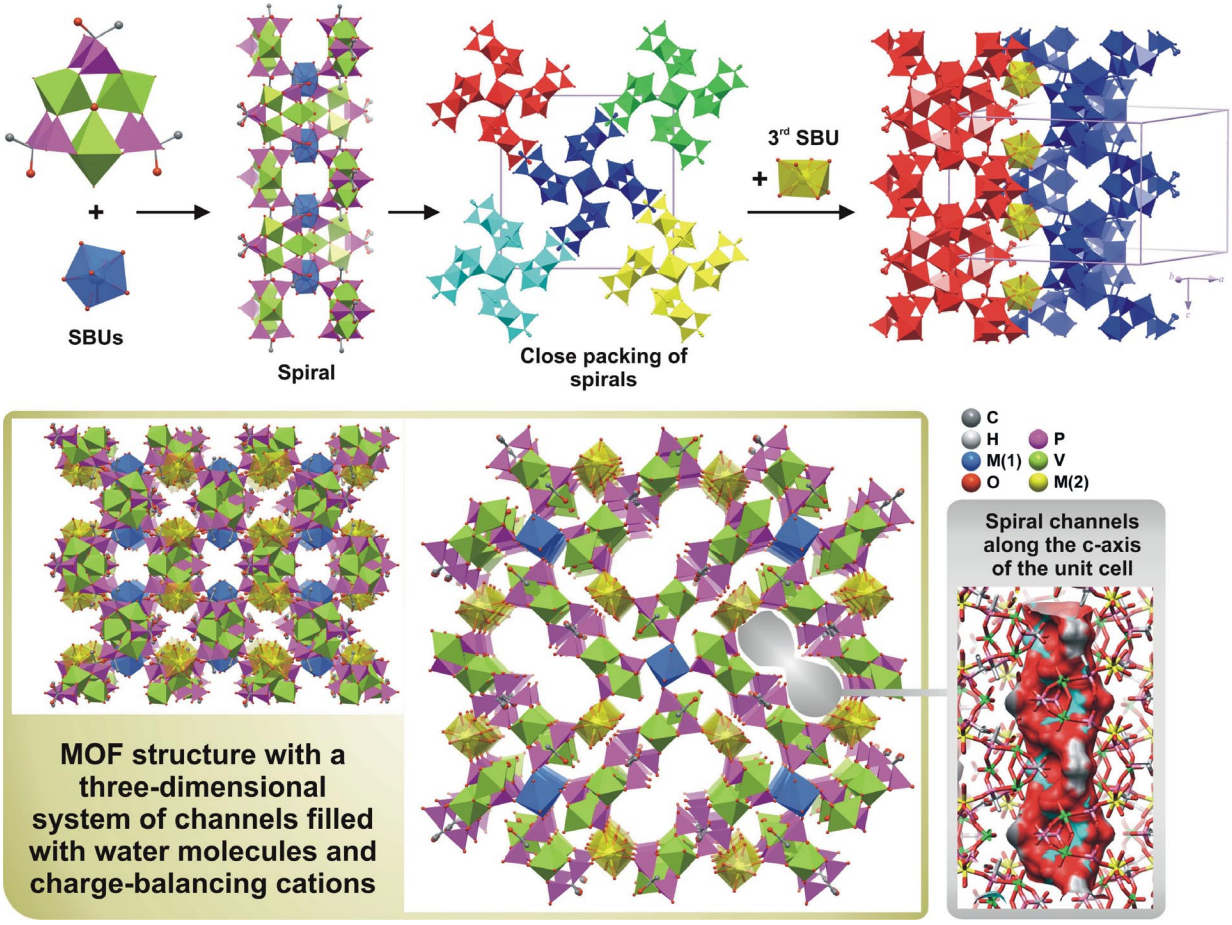

Figure 5. Modular assembly of the SBUs to form the anionic $_\infty{}^3[M_{12}V_{24}O_{24}(OH)_8(H_2hedp)_8(Hhedp)_{16}(H_2O)_{64+n}]^{12-}$ frameworks.

Connectivity of the $[V_3O_3(OH)(H_2hedp)(Hhedp)_2]^{6-}$ Building Block and Modular Framework Construction

The most important prerequisite for the classification of a MOF as a modular structure is the ability of the constituent building blocks to exist as separate entities, in solution or in the solid state. Indeed, all molecular entities described in the previous subsections exist in such a form (e.g. lanthanide cations are present in solution as aqua complexes), thus supporting the classification of the materials here described as modular.

Figures 5 and 6 show schematically how the frameworks may self-assemble from the individual SBUs; the pivotal "brick" is the trinuclear $[V_3O_3(OH)(H_2hedp)(Hhedp)_2]^{6-}$ units. Firstly, the latter and the dodecahedral M(1) centres organize in spirals along the [001] direction of the unit cell, and the connectivity imposes M(1)···M(1) inter-lanthanide distances in the range 8.0082(1)–8.1203(3) Å (**1s**, **2s** and **6s**). Secondly, individual, symmetry-related spirals organize themselves in the crystal structures in a brick-wall fashion in the *ab* plane of the unit cell and are structurally connected to each other through the M(2) centres [M(2)···M(2) distances also in the 8.0082(1)–8.1203(3) Å range]. We believe that this self-assembly process occurs as a whole – the spirals and framework form at the same time.

The relatively large size of the trinuclear $[V_3O_3(OH)(H_2hedp)(Hhedp)_2]^{6-}$ units results in large voids in the resulting frameworks, which leads to the existence of various types of channels, the most prominent of which runs parallel to the *c* axis (Figure 5) and contains a large number of highly disordered water molecules (see Experimental Section dedicated to single-crystal X-ray diffraction studies for further details on the water content). This self-assembly occurs at ambient temperature, just by magnetically stirring the reactants, but at the expense of the crystallinity of the materials (Figures S4–S8 in the Supporting Information).

Charge-Balance of the Lanthanide Cations

The aforementioned connectivity leads to the formation of anionic MOF compounds with the general formula $_\infty^3[M_{12}V_{24}O_{24}(OH)_8(H_2hedp)_8(Hhedp)_{16}(H_2O)_{64+n}]^{12-}$. There are a number of lanthanide cations that balance the crystal

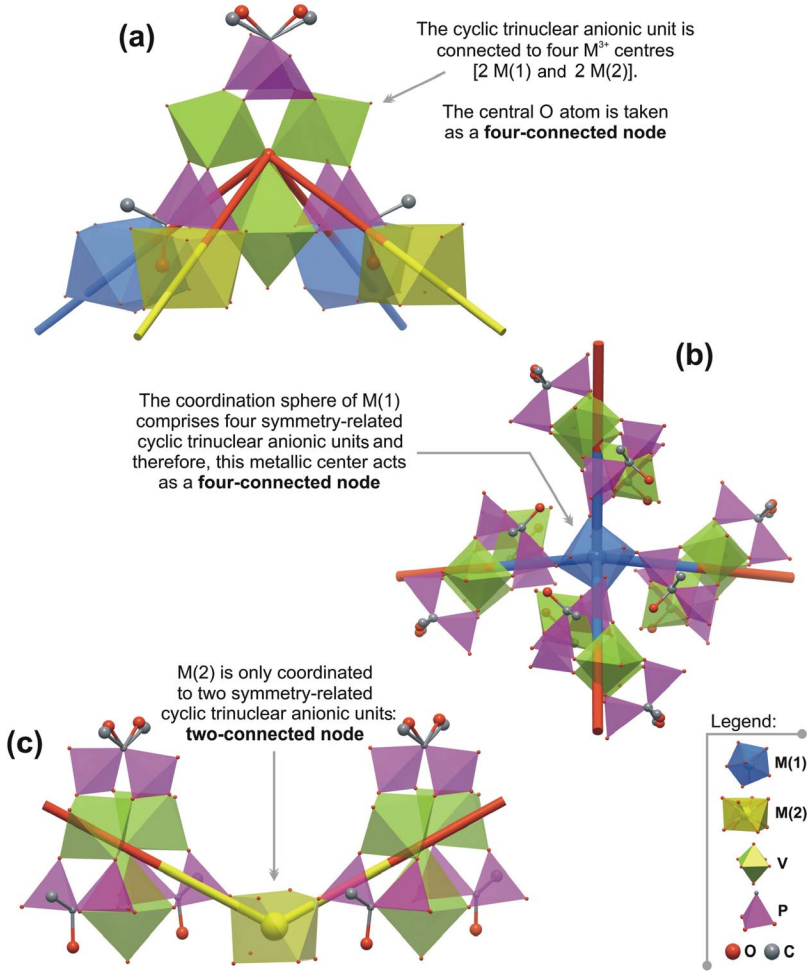

Figure 6. Schematic representation of the connectivity of the nodes forming the anionic $_\infty^3[M_{12}V_{24}O_{24}(OH)_8(H_2hedp)_8(Hhedp)_{16}(H_2O)_{64+n}]^{12-}$ framework: the central oxygen atom of the cyclic trinuclear anionic building block and the M(1) centres act as four-connected nodes, while M(2) are two-connected nodes.

charge within the spiral channels running parallel to *c* axis of the unit cell (Figure 5). These are highly disordered cations, and no specific coordination environment could be ascribed to each crystallographic position (further details on the location and refinement of these charge-balancing cations are provided in the Experimental Section dedicated to single-crystal X-ray structure solution and refinement).

Topological Analysis of the $_{\infty}^{3}[M_{12}V_{24}O_{24}(OH)_8(H_2hedp)_8(Hhedp)_{16}(H_2O)_{64+n}]^{12-}$ Framework

The SBU connectivity is more clearly described by using a typical topological approach in which the network is progressively reduced to simple central nodes and bridging rods.[22] All topological studies have been performed by using the software package TOPOS.[23] Because each SBU seems to exist as an independent entity in solution and it is feasible to assume that crystal growth occurs preferentially at the expense of the addition of each "brick" to the existing crystallites, each type of unit should be considered as an individual node of the MOF network. In this sense, the structure is trinodal (Figures 6 and 7): the trinuclear $[V_3O_3(OH)(H_2hedp)(Hhedp)_2]^{6-}$ unit is connected to four lanthanide centres (4-connected node, Figure 6a), while M(1) and M(2) bridge 4 and 2 anionic units, respectively, (4- and 2-connected nodes, Figure 6b, c). The total Schäfli symbol is $\{4.8^3.10^2\}_2\{4^2.8^4\}\{8\}_2$, which was identified by TOPOS as an unprecedented topology. This was further confirmed by systematic searches in *Reticular Chemistry Structure Resource* (RCSR)[24] and EPINET (Figure 7).[25]

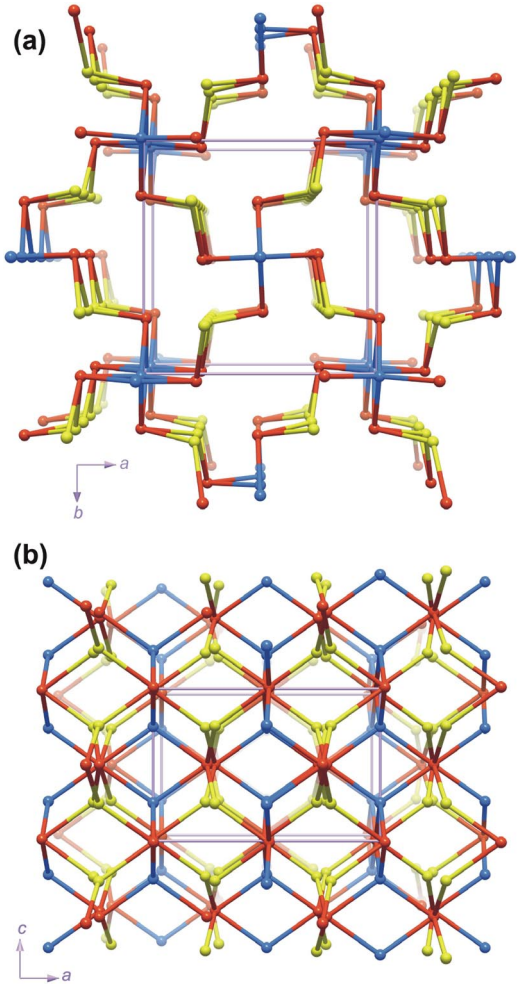

Figure 7. Topological representations of the anionic $_{\infty}^{3}[M_{12}V_{24}O_{24}(OH)_8(H_2hedp)_8(Hhedp)_{16}(H_2O)_{64+n}]^{12-}$ frameworks viewed along the (a) [001] and (b) [010] directions of the unit cell.

FTIR

FTIR studies have been performed on microcrystalline powders $M_4[M_{12}V_{24}O_{24}(OH)_8(H_2hedp)_8(Hhedp)_{16}(H_2O)_{64+n}]\cdot 88+y(H_2O)$ [where M^{3+} = Y^{3+} (**1**), Ce^{3+} (**2**), Sm^{3+} (**3**), Eu^{3+} (**4**) and Tb^{3+} (**5**)] and single-crystals of $Er_4[Er_{12}V_{24}O_{24}(OH)_8(H_2hedp)_8(Hhedp)_{16}(H_2O)_{64}]\cdot 88+y(H_2O)$ (**6s**). Spectra are almost identical for all compounds and exhibit the main diagnostic bands of the primary building blocks (Figure S9 in the Supporting Information).[26]

The extensive hydrogen-bonding network involving coordinated and uncoordinated water molecules materializes in the FTIR spectra through the presence of the typical υ(O–H) stretching vibrational modes [very broad band(s) above 3000 cm^{-1}, not shown] and the δ(O–H···O) and γ(O–H···O) modes at 1338 and 927 cm^{-1}, respectively. Moreover, the large amount of water also gives rise to a very broad band at ca. 1640 cm^{-1} with medium-to-strong intensity [δ(H–O–H)] as a result of the in-plane deformation of the water molecules .

The presence of coordinated anionic $H_{5-x}hedp^{-x}$ residues is also clearly visible, particularly below 2000 cm^{-1}. The υ(P=O) stretching vibrational mode appears broadened and as a redshifted shoulder at 1175 cm^{-1}, relative to the analogous band for the uncoordinated molecule. This is attributed to the combined effect of coordination to the M^{3+} cations (which significantly weakens the P^+–O^- bond) and the presence of strong hydrogen bonds with water molecules.[26] The coordination of $H_{5-x}hedp^{-x}$ to M^{3+} is reflected in the typical symmetrical [$\upsilon_{sym}(PO_2)$] and asymmetrical [$\upsilon_{asym}(PO_2)$] stretching vibrational modes of the phosphonate groups, which appear as very strong bands at 1015 and 1105 cm^{-1}, respectively; the former is significantly shifted to the red relative to the band of the same vibration for the uncoordinated organic molecule (ca. 1063 cm^{-1}). All spectra indicate that the substituent methyl groups belong to the $H_{5-x}hedp^{-x}$ residues through the bands at 1454 and 1378 cm^{-1}, respectively, typical of $\delta_{sym}(C–CH_3)$ and $\delta_{asym}(C–CH_3)$ deformations.

The crystallographic assumption of the presence of protonated $H_{5-x}hedp^{-x}$ residues within the cyclic trinuclear anionic unit $[V_3O_3(OH)(H_2hedp)(Hhedp)_2]^{6-}$ to balance the crystal charge is confirmed by FTIR spectroscopy. Indeed, as previously reported by Afonin et.al,[27] a medium-intensity band assigned to the typical υ(P–O–H) stretching vibration is located at 912 cm^{-1}.

Some important structural arrangements of the cyclic anionic unit are further observed at low wavenumbers: while a very broad and strong band observed at 650–550 cm^{-1} is associated with typical V–O–V stretching vibrational modes, the band at 979 cm^{-1} may encompass the ν(V=O) vibration.

Thermogravimetry and Variable-Temperature Powder X-ray Diffraction

The thermal stabilities of **1**–**5** and single-crystals of **6s** have been investigated by combining thermogravimetry (Figure S10) and variable-temperature powder X-ray diffraction (VTPXRD) (Figure S11). All compounds exhibit similar thermal stabilities. Zeolite-type weight losses under 100 °C are attributed to the release of most water molecules residing in the channels and many of those coordinated to the lanthanide centres. However, VTPXRD of **6s** shows that this release results in the collapse of the framework, a process that settles in before 100 °C and is essentially terminated at ca. 200 °C (Figure S11). In accord, the majority of the weight loss occurs before 200 °C (Figure S10), which leads to almost amorphous materials that preserve their identity until ca. 600 °C. After the latter temperature, additional weight loss is observed, which leads to the formation of inorganic crystalline phases, present at 800 °C (Figure S11).

Photoluminescence Properties

Figure 8a shows the room temperature emission spectra of **4** under UV excitation. The spectra display a broad band at 380–580 nm, superimposed on both the intra-$4f^6$ self-absorption bands attributed to the $^7F_{0,1}\rightarrow{}^5D_2$ transitions and a series of Eu^{3+}-intra-$4f^6$ lines ascribed to the $^5D_1\rightarrow{}^7F_1$ and $^5D_0\rightarrow{}^7F_{0-4}$ transitions. The broad band is ascribed to the V=O bond.[28] The intra-$4f^6$ self-absorption suggests the presence of radiative vanadium-to-Eu^{3+} energy transfer. By increasing the excitation wavelength from 290 nm to 350 nm, the relative intensity of the vanadium-related band increases and the energy, full-width-at-half-maximum (fwhm) and number of Stark components of the Eu^{3+}-intra-$4f^6$ lines change (see below). The selective excitation paths for the vanadium and Eu^{3+}-related emission were studied through the acquisition of excitation spectra while monitoring both the broad band emission (at 460 nm) and the $^5D_0\rightarrow{}^7F_2$ transition (619 nm). The former spectrum displays a broad charge-transfer (CT) band, which arises from electron transfer from the oxygen to the V^{4+} ions.[28] Intra-$4f^6$ self-absorption bands attributed to the $^7F_{0,1}\rightarrow{}^5L_6$ transitions are also observed. The excitation spectrum monitored within the Eu^{3+} emission lines consists of a broad band with two components at 290 and 350 nm, attributed to the Eu–O CT bands,[29] and low intensity intra-$4f^6$ peaks, ascribed to the $^7F_{0,1}\rightarrow{}^5L_6$ transitions. The low relative intensity of the intra-$4f^6$ lines points out that the Eu^{3+} excited states are essentially populated through the CT bands, rather than by direct intra-$4f^6$ excitation.

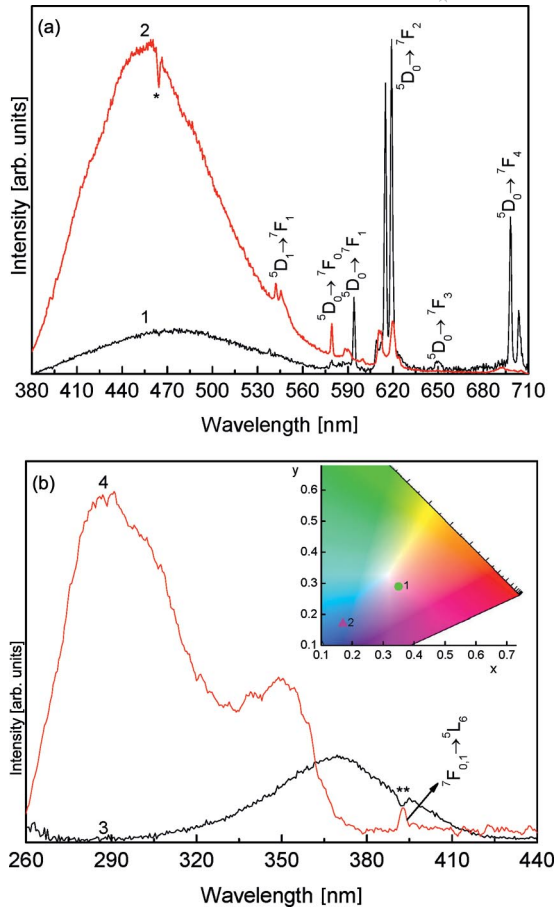

Figure 8. Room temperature (a) emission spectra excited at 290 nm (1) and 350 nm (2). (b) Excitation spectra monitored at 460 nm (3) and 619 nm (4) for compound **4**. * and ** depict the Eu^{3+}-intra-$4f^6$ $^7F_{0,1}\rightarrow{}^5D_2$ and the $^7F_{0,1}\rightarrow{}^5L_6$ self-absorptions, respectively. The inset displays a partial CIE chromatic diagram (1931) showing the (x,y) colour coordinates of the room temperature emission excited at 290 nm (1) and 350 nm (2).

Because the vanadium-related emission overlaps with the Eu^{3+} intra-$4f^6$ emission, the colour may easily be tuned from white (0.35,0.29) to purplish-blue (0.17,0.17) by changing the excitation wavelength, as illustrated in the partial CIE chromaticity diagram (inset in Figure 8b).

In order to get a better insight into the Eu^{3+} emission features, the $^5D_0\rightarrow{}^7F_{0-4}$ transitions were scanned with higher resolution at two selected excitation wavelengths (Figure 9). With excitation at 290 nm, a single component is observed with very low relative intensity for the non-degenerated $^5D_0\rightarrow{}^7F_0$ transition and 1 and 2 Stark components are observed for the $^5D_0\rightarrow{}^7F_{1,2}$ transitions, respectively (marked with arrows in Figure 9c–d). By increasing the excitation wavelength, and despite having the same energy, the relative intensity of the non-degenerated $^5D_0\rightarrow{}^7F_0$ transition increases by one order of magnitude and, at least, 5 and 7 Stark components are detected for the $^5D_0\rightarrow{}^7F_{1,2}$ transitions, respectively (marked with arrows in Figure 9c–d). The Eu^{3+} emission dependence on the excitation wavelength and the Stark splitting of the $^5D_0\rightarrow{}^7F_{1,2}$ transitions, whose maximum allowed splitting is 3 and 5, respectively,

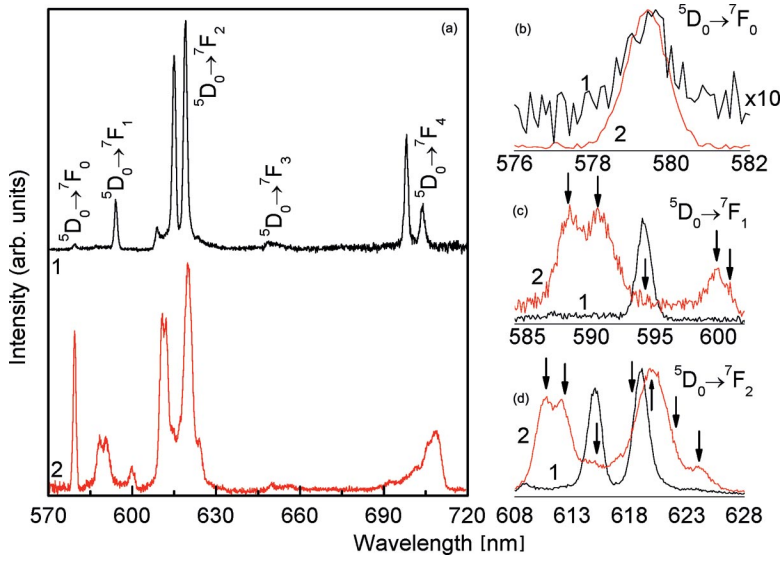

Figure 9. (A) High-resolution room temperature emission spectra excited at 290 nm (1) and 350 nm (2) for compound **4**. (b)–(d) show a magnification of the $^7D_0\rightarrow{}^7F_{0-2}$ transitions, respectively.

arises from the presence of more than one Eu^{3+} average local environment, in accord with the crystallographic studies.

Lowering of the temperature to 12 K (which requires high-vacuum pumping) results in a decrease in the emission intensity (most evident for the Eu^{3+} $^5D_0\rightarrow{}^7F_{0-4}$ transitions, relative to that of the vanadium-related component). This is presumably due to a loss of crystallinity brought about by (at least) partial framework collapse caused by the removal of the water molecules of crystallization.

Conclusion

The cyclic trinuclear $[V_3O_3(OH)(H_2hedp)(Hhedp)_2]^{6-}$ unit, previously reported by Aleksandrov et al., seems to spontaneously form in aqueous solution at ambient temperature. This unit is a robust building block for the construction of modular mixed-metal–organic frameworks containing V^{4+} ions and trivalent lanthanide centres, $M_4[M_{12}V_{24}O_{24}(OH)_8(H_2hedp)_8(Hhedp)_{16}(H_2O)_{64+n}]\cdot 88+y(H_2O)$. New compounds were isolated, both as large-single crystals from the slow evaporation of the solvent (for Y^{3+}, Ce^{3+} and Er^{3+}) and microcrystalline powders by magnetically stirring overnight (one-pot synthesis of Y^{3+}, Ce^{3+}, Sm^{3+}, Eu^{3+}, Tb^{3+} and Gd^{3+} materials). Although the latter route affords less crystalline materials, the reaction period is reduced from weeks/months to hours, and the yield is improved.

The self-assembly of the frameworks is a direct consequence of their modular nature (secondary building units – cyclic trinuclear anionic unit and two lanthanide aqua complexes). The large size of the anionic unit seems to direct the formation of large channels housing highly disordered water molecules. Despite the fact that the framework collapses at mild temperatures, these materials are reminiscent of zeolites, and the majority of the solvent molecules are released below 100 °C.

The reported materials exhibit interesting photoluminescence properties. Notably, the simultaneous presence of V^{4+} and Eu^{3+} centres allows a fine tuning of the photoluminescence: by simply changing the excitation wavelength, the emission is tuned from white to purplish-blue.

Experimental Section

General Instrumentation: Sample morphology and identification of the main constituent elements (EDS) were performed on a Low Vacuum Scanning Electron Microscope operating at 25 kV, FEG-SEM Hitachi S-4100, equipped with an energy dispersive X-ray analysis Römteck System with polymeric window. Samples were fixed in aluminium holders with adhesive carbon foil and were carbon coated. FTIR spectra were collected by using KBr pellets (Aldrich, 99%+, FTIR grade) on a Mattson 7000 FTIR spectrometer. Thermogravimetric analysis (TGA) was carried out on a Shimadzu TGA-50, with a heating rate of 10 °C/min, under a nitrogen atmosphere with a flow rate of 20 cm^3/min. Elemental CH analyses were performed with a FISONS EA1108 instrument. Optical photographs were taken with a Stemi 2000 stereomicroscope equipped with Carl Zeiss lenses and a digital high-resolution AxioCam MRc5 digital camera connected to a personal computer. Variable-temperature powder X-ray diffraction data for $Er_4[Er_{12}V_{24}O_{24}(OH)_8(H_2hedp)_8(Hhedp)_{16}(H_2O)_{64}]\cdot 88+y(H_2O)$ (**6s**) were collected on a X′Pert MPD Philips diffractometer (Cu-K_α X-radiation, λ = 1.54060 Å), equipped with a X′Celerator detector, curved graphite-monochromated radiation, a flat-plate sample holder in a Bragg–Brentano para-focusing optics configuration (40 kV, 50 mA), and a high-temperature Antoon Parr HKL 16 chamber controlled by a Antoon Parr 100 TCU unit. Intensity data were collected in the step mode (0.05°, 1 s per step) in the range ca. $4 \leq 2\theta \leq 36°$. Chemicals were readily available from commercial sources and used as received without further purification: 1-hydroxyethylidenediphosphonic acid (etidronic acid, H_5hedp) tetrasodium salt (Na_4Hhedp, $C_2H_4Na_4O_7P_2$, ≥90% Fluka), vanadium(IV) oxide sulfate pentahy-

drate ($VOSO_4{\cdot}5H_2O$, 99% Sigma–Aldrich), malonic acid ($C_3H_4O_4$, 99% Merck–Schuchardt), oxalic acid dihydrate ($H_2C_2O_4{\cdot}H_2O$, 99%, Panreac), cerium(III) chloride heptahydrate ($CeCl_3{\cdot}7H_2O$,≥98.5% Fluka), samarium(III) chloride hexahydrate ($SmCl_3{\cdot}6H_2O$,≥99% Aldrich), europium(III) chloride hexahydrate ($EuCl_3{\cdot}6H_2O$,≥99.9% Aldrich), terbium(III) chloride hexahydrate ($TbCl_3{\cdot}6H_2O$,≥99.9% Aldrich), yttrium(III) chloride hexahydrate ($YCl_3{\cdot}6H_2O$,≥99.9% Aldrich), erbium(III) chloride hexahydrate ($ErCl_3{\cdot}6H_2O$,≥99.9% Aldrich) and gadolinium(III) chloride hexahydrate ($GdCl_3{\cdot}6H_2O$,≥99.9% Aldrich).

Synthesis of Single-crystals of $M_4[M_{12}V_{24}O_{24}(OH)_8(H_2hedp)_8(Hhedp)_{16}(H_2O)_{64+n}]{\cdot}88+y(H_2O)$, $M^{3+} = Y^{3+}$ (1s), Ce^{3+} (2s) ($n = 8$ for 2s): A mixture containing Na_4Hhedp (0.180 g), $C_3H_4O_4$ (0.140 g), $VOSO_4{\cdot}5H_2O$ (0.100 g) and $CeCl_3{\cdot}7H_2O$ (0.460 g) in distilled water (ca. 5 g) was stirred thoroughly for 30 min at ambient temperature to yield a homogeneous suspension, with a molar composition of 1.18:2.19:1.00:2.01:45.28, respectively. This mixture was then transferred into a PTFE-lined Parr Instruments stainless steel reaction vessel (ca. 10 cm^3), which was then placed inside a pre-heated oven at 180 °C for a period of 72 h. After the reaction, the vessel was removed and left to cool to ambient temperature before opening. A blue aqueous solution was then isolated by filtering a small amount of a white powder, which was then left to stand at ambient temperature. After one week, large light-blue single-crystals of **2s** were manually harvested from the bottom and walls of the vial. The preparation of **1s** followed the same experimental procedure but instead $YCl_3{\cdot}6H_2O$ (0.370 g) was used.

Synthesis of Single-crystals of $Er_4[Er_{12}V_{24}O_{24}(OH)_8(H_2hedp)_8(Hhedp)_{16}(H_2O)_{64}]{\cdot}88+y(H_2O)$ (6s): A mixture containing Na_4Hhedp (0.150 g), $VOSO_4{\cdot}5H_2O$ (0.100 g) and $ErCl_3{\cdot}6H_2O$ (0.260 g) was dissolved in distilled water (ca. 6.5 g) under continuous and vigorous magnetic stirring at ambient temperature. The pH of the reaction mixture was adjusted to ca. 1 by adding oxalic acid (0.08 g). The resulting mixture was then transferred into a PTFE-lined Parr Instruments stainless steel reaction vessel (ca. 10 cm^3) and placed inside a preheated oven at 150 °C over a period of 72 h. After the reaction, the vessel was allowed to cool slowly to ambient temperature before opening. A blue powder was found at the bottom of the reaction vessel and easily separated by filtration. The light-blue mother liquor was moved to a clean glass tube, and the solvent was allowed to evaporate slowly over one month, which resulted in a large quantity of well-shaped, light-blue single-crystals suitable for single-crystal X-ray analysis. Selected FTIR data: υ(O–H, water) ≈ 3680–3140 (vs br.), δ(H–O–H, water) = 1639 (vs), $\delta_{asym}(C–CH_3)$ = 1450 (w), $\delta_{sym}(C–CH_3)$ = 1383 (w), δ(O–H···O) = 1330 (w br.), υ(P=O) = 1178 (s sh.), $\upsilon_{asym}(P–O_{coord})$ = 1112 (vs br.), $\upsilon_{sym}(P–O_{coord})$ = 1018 (vs), υ(V=O) = 981 (s sh.), υ(P–O–H) and γ(O–H···O) = 928 (m) and 909 (m), υ(P–O) and υ(P–C) = 822 (m br.), υ(V–O–V) = 605 (s br.) cm^{-1}. TGA data (weight loss in %) and derivative thermogravimetric peak (DTG, in italics inside the parentheses): 24–700 °C – 31.6% (*82 °C*). EDS Er/V/P molar ratio = 1:1.4:3.8. Elemental Analysis (in%): found C 4.82, H 3.90.

Facile One-Pot Synthesis at Ambient Temperature of Microcrystalline Powders

$M_4[M_{12}V_{24}O_{24}(OH)_8(H_2hedp)_8(Hhedp)_{16}(H_2O)_{64+n}]{\cdot}88+y(H_2O)$ (1–7): Microcrystalline powder samples of $M_4[M_{12}V_{24}O_{24}(OH)_8(H_2hedp)_8(Hhedp)_{16}(H_2O)_{64+n}]{\cdot}88+y(H_2O)$ [$M^{3+} = Y^{3+}$ (**1**), Ce^{3+} (**2**), Sm^{3+} (**3**), Eu^{3+} (**4**), Tb^{3+} (**5**) and Gd^{3+} (**7**)] were readily synthesized by one-pot synthesis at ambient temperature, with vigorous magnetic stirring and from reaction mixtures in distilled water. Typically, in order to isolate compound **2** Na_4Hhedp (0.600 g), $C_3H_4O_4$ (0.580 g), $VOSO_4{\cdot}5H_2O$ (0.600 g) and $CeCl_3{\cdot}7H_2O$ (0.138 g) were mixed in distilled water (ca. 50 g), and the mixture was magnetically stirred thoroughly overnight, which led to a heterogeneous mixture from which a large quantity of a microcrystalline blue powder (ca. 0.67 g) was isolated by filtration. This was then washed with copious amounts of distilled water and dried in air at 70 °C. The remaining compounds were isolated through similar experimental procedures by using $YCl_3{\cdot}6H_2O$ (1.110 g), $SmCl_3{\cdot}6H_2O$ (1.350 g), $EuCl_3{\cdot}6H_2O$ (1.350 g), $TbCl_3{\cdot}6H_2O$ (1.400 g), $GdCl_3{\cdot}6H_2O$ (1.50 g), respectively, instead of $CeCl_3{\cdot}7H_2O$.

Compound 1: Selected FTIR data: υ(O–H, water) ≈ 3600–3150 (vs br.), δ(H–O–H, water) = 1643 (vs), $\delta_{asym}(C–CH_3)$ = 1452 (w), $\delta_{sym}(C–CH_3)$ = 1377 (w), δ(O–H···O) = 1338 (w br.), υ(P=O) = 1176 (s sh.), $\upsilon_{asym}(P–O_{coord})$ = 1115 (vs br.), $\upsilon_{sym}(P–O_{coord})$ = 1018 (vs), υ(V=O) = 982 (s sh.), υ(P–O–H) and γ(O–H···O) = 927 (m) and 911 (m), υ(P–O) and υ(P–C) = 824 (m br.), υ(V–O–V) = 607 (s br.) cm^{-1}. TGA data (weight loss in %) and derivative thermogravimetric peaks (DTG, in italics inside the parentheses): 34–525 °C – 32.8% (*87* and *301 °C*), 525–800 °C – 4.7% (*634 °C*). EDS Y:V:P molar ratio = 1:1.6:2.3. Elemental Analysis (in%): found C 4.35, H 4.28.

Compound 2: Selected FTIR data: υ(O–H, water) ≈ 3615–3100 (vs br.), δ(H–O–H, water) = 1638 (vs), $\delta_{asym}(C–CH_3)$ = 1454 (w), $\delta_{sym}(C–CH_3)$ = 1375 (w), δ(O–H···O) = 1332 (w br.), υ(P=O) = 1172 (s sh.), $\upsilon_{asym}(P–O_{coord})$ = 1110 (vs br.), $\upsilon_{sym}(P–O_{coord})$ = 1012 (vs), υ(V=O) = 974 (s sh.), υ(P–O–H) and γ(O–H···O) = 928 (m) and 912 (m), υ(P–O) and υ(P–C) = 825 (m br.), υ(V–O–V) = 604 (s br.) cm^{-1}. TGA data (weight loss in %) and derivative thermogravimetric peaks (DTG, in italics inside the parentheses): 23–600 °C – 30.4% (*67 °C*), 600–900 °C – 3.6% (*757 °C*). EDS Ce:V:P molar ratio = 1:1.4:2.3. Elemental Analysis (in%): found C 3.34, H 3.19.

Compound 3: Selected FTIR data: υ(O–H, water) ≈ 3550–3158 (vs br.), δ(H–O–H, water) = 1641 (vs), $\delta_{asym}(C–CH_3)$ = 1453 (w), $\delta_{sym}(C–CH_3)$ = 1377 (w), δ(O–H···O) = 1334 (w br.), υ(P=O) = 1171 (s sh.), $\upsilon_{asym}(P–O_{coord})$ = 1107 (vs br.), $\upsilon_{sym}(P–O_{coord})$ = 1014 (vs), υ(V=O) = 977 (s sh.), υ(P–O–H) and γ(O–H···O) = 926 (m) and 912 (m), υ(P–O) and υ(P–C) = 824 (m br.), υ(V–O–V) = 605 (s br.) cm^{-1}. TGA data (weight loss in %) and derivative thermogravimetric peaks (DTG, in italics inside the parentheses): 25–550 °C – 30.5% (*82 °C*), 550–750 °C – 3.7% (*681 °C*). EDS Sm:V:P molar ratio = 1:1.4:2.8. Elemental Analysis (in %): found C 4.18, H 3.81.

Compound 4: Selected FTIR data: υ(O–H, water) ≈ 3520–3175 (vs br.), δ(H–O–H, water) = 1642 (vs), $\delta_{asym}(C–CH_3)$ = 1454 (w), $\delta_{sym}(C–CH_3)$ = 1379 (w), δ(O–H···O) = 1336 (w br.), υ(P=O) = 1172 (s sh.), $\upsilon_{asym}(P–O_{coord})$ = 1107 (vs br.), $\upsilon_{sym}(P–O_{coord})$ = 1015 (vs), υ(V=O) = 975 (s sh.), υ(P–O–H) and γ(O–H···O) = 929 (m) and 912 (m), υ(P–O) and υ(P–C) = 823 (m br.), υ(V–O–V) = 602 (s br.) cm^{-1}. TGA data (weight loss in %) and derivative thermogravimetric peaks (DTG, in italics inside the parentheses): 24–600 °C – 28.4% (*72* and *134 °C*), 600–1000 °C – 3.6% (*774 °C*). EDS Eu:V:P molar ratio = 1:1.5:2.9. Elemental Analysis (in%): found C 4.18, H 4.11.

Compound 5: Selected FTIR data: υ(O–H, water) ≈ 3550–3195 (vs br.), δ(H–O–H, water) = 1642 (vs), $\delta_{asym}(C–CH_3)$ = 1454 (w), $\delta_{sym}(C–CH_3)$ = 1378 (w), δ(O–H···O) = 1336 (w br.), υ(P=O) = 1178 (s sh.), $\upsilon_{asym}(P–O_{coord})$ = 1110 (vs br.), $\upsilon_{sym}(P–O_{coord})$ = 1016 (vs), υ(V=O) = 977 (s sh.), υ(P–O–H) and γ(O–H···O) = 929 (m) and 912 (m), υ(P–O) and υ(P–C) = 824 (m br.), υ(V–O–V) = 605 (s br.) cm^{-1}. TGA data (weight loss in %) and derivative thermogravimetric peaks (DTG, in italics inside the parentheses): 23–500 °C – 29.9% (*82* and *316 °C*), 500–1000 °C – 3.7% (*690 °C*). EDS Y:V:P

molar ratio = 1:1.4:3.7. Elemental Analysis (in%): found C 4.00, H 3.83.

Single-Crystal X-ray Diffraction Studies of $M_4[M_{12}V_{24}O_{24}(OH)_8(H_2hedp)_8(Hhedp)_{16}(H_2O)_{64+n}]\cdot 88+y(H_2O)$, M^{3+} = Y^{3+} (1s), Ce^{3+} (2s), Er^{3+} (6s) (n = 8 for 2s): Suitable single-crystals were manually harvested and mounted on Hampton Research CryoLoops (Figures S1–S3) by using FOMBLIN Y perfluoropolyether vacuum oil (LVAC 25/6), purchased from Aldrich. A Stemi 2000 stereomicroscope equipped with Carl Zeiss lenses were used.[30] It is important to note that although crystals of **6s** (Figure S3) were manually selected from the crystallization vial while still immersed in the mother liquor, crystals of **1s** (Figure S1) and **2s** (Figure S2) were previously dried in open air and at ambient temperature. Visual inspection under an optical microscope showed that crystal integrity was slightly compromised for **1s** and **2s**, with a number of cracks clearly visible on each individual crystal, in particular for the latter compound as indicated by SEM analysis (Figure S2). Nevertheless, preliminary single-crystal measurements of different batch crystals consistently gave the same primitive tetragonal unit cell as that registered for **6s**. Complete single-crystal data sets were collected at 150(2) K on a Bruker X8 Kappa APEX II charge-coupled device (CCD) area-detector diffractometer (Mo-K_α graphite-monochromated radiation, λ = 0.7107 Å) controlled by the APEX2 software package[31] and equipped with an Oxford Cryosystems Series 700 cryostream monitored remotely by using the software interface Cryopad.[32] Images were processed with the software package SAINT+,[33] and data were corrected for absorption by the multiscan semiempirical method implemented in SADABS.[34]

The XPREP interface was used to analyze data symmetry for the subsequent crystal solution and refinement steps. Systematic absences suggested two candidate space groups, $P4_2bc$ and $P4_2/mbc$, both having low figures of merit, for the three single-crystal data sets. By considering the calculated mean $|E^2 - 1|$ value, the latter space group was chosen for structure solution by using the Patterson synthesis algorithm implemented in SHELXS-97,[35] which allowed the immediate location of the majority of the heavy metallic centres, particularly the M^{3+} and V^{4+} that compose the anionic three-dimensional framework. All the remaining non-hydrogen atoms were located from difference Fourier maps calculated from successive full-matrix least-squares refinement cycles on F^2 by using SHELXL-97[36] and, when appropriate, refined successfully by using anisotropic displacement parameters. As a result of the likely loss of solvent from the channels in the structure (as registered, for example, for compound **2s** – see Figure S2), which can be accompanied by a possible decrease in overall symmetry, crystal solution in the non-centrosymmetric $P4_2$bc space group was also attempted for the three data sets. However, no significant improvement in the quality of the final refined model was observed, and investigations for the presence of additional symmetry elements with PLATON[37] further suggested a change in the space group to $P4_2/mbc$.

Tetragonal unit cells are also known to exhibit twinning by merohedry.[38] Preliminary studies that uses the XPREP interface for the three collected data sets revealed the possibility of such an occurrence, and the twin law [010 100 00–1] was implemented in intermediate stages of the refinement processes along with one BASF parameter. After several cycles of least-squares refinements, the quality of the crystal solution did not improve, and very large s.u.s were registered for the BASF parameter, which ultimately suggested that the structure is in fact not twinned. This was further confirmed by using the program ROTAX[39] (available with the software package CRYSTALS),[40] and also the TWINROTMAT routines implemented in PLATON.[37]

The three crystal structures contain a common cyclic trinuclear anionic unit, $[V_3O_3(OH)(H_2hedp)(Hhedp)_2]^{6-}$, which shares striking similarities with that previously described by Aleksandrov et al.[20] a few years ago. However, in that initial report this anionic unit exhibited a sixfold inversion symmetry (i.e. one V^{4+} and one $H_{5-x}hedp^{-x}$ in the asymmetric unit), while in the present structure, the overall symmetry is reduced to a mirror plane. Consequently, the asymmetric unit of **1s**, **2s** and **6s** contains two crystallographically independent V^{4+} centres and another two $H_{5-x}hedp^{-x}$ residues; each moiety is only half occupied. Moreover, as also described by Aleksandrov et al. in their crystal structure, the V^{4+} centres were also found to be markedly affected by statistical positional disorder occupying either the *exo* [V(1) or V(2)] or the *endo* [V(1′) or V(2′)] positions in the cyclic unit (see Figure S9). While in that previous report the ratio was fixed at $^2/_3$:$^1/_3$ for the *exo*/*endo* V^{4+} crystallographic positions, respectively, the good quality of the data sets for compounds **1s**, **2s** and **6s** allowed a sensible free refinement of the rates of occupancy for each pair of disorder centres, which ultimately converged to the values summarized in Figure 1. For the $H_{5-x}hedp^{-x}$ residue generated by mirror symmetry, the –OH and $–CH_3$ moieties attached to the central carbon atom were found to be disordered and were included in the final structural model with a fixed rate of occupancy of 50% for each. Moreover, in order to ensure chemically reasonable bond lengths for these moieties, all C–OH and C–CH_3 bond lengths were restrained to common refineable values, which ultimately converged to 1.43(1) and 1.54(1) Å, respectively. Carbon and oxygen atoms associated with these disordered chemical moieties were refined in all structures with independent isotropic displacement parameters.

In the course of the structure refinement for **1s**, **2s** and **6s**, a considerable smeared-out electron density was found to be located around the special (1/2, 0, 0) crystallographic position. Initial attempts to model this electron density by assuming the presence of highly disordered water molecules of crystallization failed to produce sensible least-squares overall refinement because of the discrepancy between F_c and F_o. By taking the EDS results for all compounds into account, which suggested the existence of additional metallic centres (see experimental section dedicated to the synthesis) and ruled out the presence of chloride or sulfate anions, the data was instead successfully treated by assuming the presence of three crystallographically independent positions for partially-occupied M^{3+} metallic centres [M(3), M(4) and M(5) – fixed rate of occupancy of $^1/_3$ for each, with a total of up to 4 M^{3+} cations per unit cell]. This data treatment further allowed a sensible anisotropic refinement of these cations.

Beside four or five metal-coordinated water molecules located for structures **1s** and **6s** or **2s**, respectively, nine more crystallographically independent water molecules (which add up to a total of five and a half molecules per asymmetric unit) were successfully located for all structures directly from difference Fourier maps calculated from successive least-squares refinement cycles. The oxygen atoms associated with these water molecules could be, in general, refined by using anisotropic displacements parameters, with the exception of those closer to the M(3), M(4) and M(5) disordered centres, which were instead included in the final structural model with independent isotropic displacement parameters. Hydrogen atoms associated with both coordinated and crystallization water molecules could not be located from difference Fourier, maps and no attempt was made to place these atoms in calculated crystallographic positions. However, these hydrogen atoms have been added to the empirical formulae of the compounds (see Table 4).

The refinement strategy described above allowed the description of virtually all electron density contained within the channels of the

Table 4. Crystal and structure refinement data for $M_4[M_{12}V_{24}O_{24}(OH)_8(H_2hedp)_8(Hhedp)_{16}(H_2O)_{64+n}]\cdot 88+y(H_2O)$ [where $M^{3+} = Y^{3+}$ (**1s**), Ce^{3+} (**2s**) and Er^{3+} (**6s**)] (n = 8 for **2s**).

	1s (Y^{3+})	**2s** (Ce^{3+})	**6s** (Er^{3+})
Formula	$C_6H_{52}O_{44}P_6V_3Y_2$	$C_6H_{54}Ce_2O_{45}P_6V_3$	$C_6H_{52}Er_2O_{44}P_6V_3$
Formula weight	1344.94	1465.37	1501.64
Temperature [K]	150(2)	150(2)	150(2)
Crystal system	tetragonal	tetragonal	tetragonal
Space group	$P4_2/mbc$	$P4_2/mbc$	$P4_2/mbc$
a [Å]	23.9796(4)	24.1073(4)	23.9118(3)
b [Å]	23.9796(4)	24.1073(4)	23.9118(3)
c [Å]	16.0716(5)	16.2406(7)	16.0164(3)
Volume [Å^3]	9241.5(4)	9438.4(5)	9157.8(2)
Z	8	8	8
D_c [g cm^{-3}]	1.933	2.062	2.178
μ(Mo-K_α) [mm^{-1}]	3.393	2.782	4.542
F(000)	5416	5800	5880
Crystal size [mm]	$0.08\times0.06\times0.04$	$0.20\times0.14\times0.10$	$0.26\times0.26\times0.15$
Crystal type	blue prisms	blue prisms	blue prisms
θ range	3.60 to 29.10	3.59 to 29.13	3.51 to 29.13
Index ranges	$-32 \le h \le 28$	$-32 \le h \le 33$	$-31 \le h \le 30$
	$-32 \le k \le 32$	$-33 \le k \le 33$	$-32 \le k \le 31$
	$-13 \le l \le 21$	$-20 \le l \le 22$	$-21 \le l \le 16$
Reflections collected	102372	143662	112097
Independent reflections	6362 (R_{int} = 0.1018)	6555 (R_{int} = 0.0377)	6342 (R_{int} = 0.0416)
Data completeness	to θ = 29.10° (99.1%)	to θ = 29.13° (99.7%)	to θ = 29.13° (99.3%)
Final R indices [$I > 2\sigma(I)$][a,b]	$R1$ = 0.0801, $wR2$ = 0.2220	$R1$ = 0.0707, $wR2$ = 0.2043	$R1$ = 0.0452, $wR2$ = 0.1320
Final R indices (all data)[a,b]	$R1$ = 0.1777, $wR2$ = 0.2737	$R1$ = 0.0853, $wR2$ = 0.2210	$R1$ = 0.0601, $wR2$ = 0.1437
Weighting scheme[c]	m = 0.1293, n = 57.7705	m = 0.1066, n = 115.2091	m = 0.0711, n = 76.9327
Largest diff. peak, hole [e Å^{-3}]	2.364, –1.278	7.219, –4.588	2.206, –1.168
CCDC deposition no.	663033	663034	663035

[a] $R1 = \Sigma||F_o|-|F_c||/\Sigma|F_o|$. [b] $wR2 = \{\Sigma[w(F_o^2 - F_c^2)^2]/\Sigma[w(F_o^2)^2]\}^{1/2}$. [c] $w = 1/[\sigma^2(F_o^2) + (mP)^2 + nP]$ where $P = (F_o^2 + 2F_c^2)/3$.

anionic framework. Indeed, the SQUEEZE[41] subroutines implemented within the software package PLATON showed that only ca.165, 150 and 181 Å^3 of potential solvent accessible volume remained within the unit cells of **1s**, **2s** and **6s**, respectively, which contains approximately 95 electrons, accounting for approximately five extra uncoordinated water molecules (not included in the structures). As a result of the small amount of unaccounted water molecules on the one hand, and the overall quality of the refined structural models (see Table 4) on the other, the calculated solvent-free reflection data files calculated with SQUEEZE were not employed in subsequent full-matrix least-squares refinement cycles on F^2.

Hydrogen atoms bound to carbon and to the –OH groups bound to the central carbon atom of $H_{5-x}hedp^{-x}$ were placed in calculated positions by using the HFIX 137 and 147 instructions in SHELXL, respectively, and refined by using a riding model with an isotropic displacement parameter fixed at 1.5 times U_{eq} for the atom to which they are attached.

Upon completion of the refinement of $M_4[M_{12}V_{24}O_{24}(OH)_8(H_2hedp)_8(Hhedp)_{16}(H_2O)_{64+n}]\cdot 88+y(H_2O)$, where $M^{3+} = Y^{3+}$ (**1s**), Ce^{3+} (**2s**) and Er^{3+} (**6s**) and n = 8 for **2s**, in $P4_2/mbc$, PLATON[37] was used to verify the correctness of the structures. No obvious space group changes were necessary. In particular, the NEWSYMM routines suggested exactly the same candidates for the space groups that XPREP found in the initial stages of the crystallographic study.

The last difference Fourier map synthesis showed: for **1s**, the highest peak (2.364 e Å^{-3}) and deepest hole (–1.278 e Å^{-3}) located at 0.86 Å from Y(3) and 0.53 Å from Y(4); for **2s**, the highest peak (7.219 e Å^{-3}) and deepest hole (–4.588 e Å^{-3}) located at 0.73 Å from Ce(2) and 0.68 Å from Ce(2); for **6s**, the highest peak (2.206 e Å^{-3}) and deepest hole (–1.168 e Å^{-3}) located at 0.92 Å from Er(3) and 0.31 Å from Er(4), respectively.

Information on crystallographic data collection and structure refinement details for $M_4[M_{12}V_{24}O_{24}(OH)_8(H_2hedp)_8(Hhedp)_{16}(H_2O)_{64+n}]\cdot 88+y(H_2O)$ [where $M^{3+} = Y^{3+}$ (**1s**), Ce^{3+} (**2s**), and Er^{3+} (**6s**)] are summarized in Table 4. Selected bond lengths and angles for the M^{3+} and V^{4+} coordination environments of all structures are supplied in Tables 1, 2, and 3.

Crystallographic data (excluding structure factors) for the structures reported in this paper have been deposited with the Cambridge Crystallographic Data Centre (deposition numbers are given in Table 4). These data can be obtained free of charge from The Cambridge Crystallographic Data Centre via www.ccdc.cam.ac.uk/data_request/cif.

Phase Identification of Microcrystalline Powders by Powder X-ray Diffraction and Electron Microscopy: Powder X-ray diffraction data (PXRD) of $M_4[M_{12}V_{24}O_{24}(OH)_8(H_2hedp)_8(Hhedp)_{16}(H_2O)_{64+n}]\cdot 88+y(H_2O)$ [where $M^{3+} = Y^{3+}$ (**1**), Ce^{3+} (**2**), Sm^{3+} (**3**), Eu^{3+} (**4**) and Tb^{3+} (**5**)] were collected at ambient temperature (ca. 298 K) on a X′Pert MPD Philips diffractometer (Cu-K_α radiation, λ = 1.54060 Å), equipped with a X′Celerator detector, curved graphite-monochromated radiation and a flat-plate sample holder, in a Bragg–Brentano para-focusing optics configuration (40 kV, 50 mA). Intensity data were collected in continuous scanning mode in the range ca. $3° \le 2\theta \le 50°$. The PXRD patterns were indexed using the automatic powder indexing program DICVOL04[42] by selecting the first most-intense and well-resolved reflections (the absolute error on each reflection was fixed at $0.03\times2\theta$). Le Bail whole powder-diffraction-pattern profile fittings (one for each material) in the space group $P4_2/mbc$ were performed with the FullProf.2k software package,[43,44] by employing a typical pseudo-Voigt peak-shape function, and, in the last stages of the fitting process, the unit cell parameters and typical profile parameters, such as scale factor, zero shift, Caglioti function values[45] and two asym-

Table 5. Crystal data for $M_4[M_{12}V_{24}O_{24}(OH)_8(H_2hedp)_8(Hhedp)_{16}(H_2O)_{64+n}]\cdot 88+y(H_2O)$ [where M^{3+} = Y^{3+} (**1**), Ce^{3+} (**2**), Sm^{3+} (**3**), Eu^{3+} (**4**) and Tb^{3+} (**5**)] (ambient temperature) from Le Bail whole powder-diffraction-pattern profile fittings.

	1 (Y^{3+})	**2** (Ce^{3+})	**3** (Sm^{3+})	**4** (Eu^{3+})	**5** (Tb^{3+})
Crystal system	tetragonal	tetragonal	tetragonal	tetragonal	tetragonal
Space group	$P4_2/mbc$	$P4_2/mbc$	$P4_2/mbc$	$P4_2$/mbc	$P4_2/mbc$
a [Å]	23.992(3)	24.085(5)	24.070(2)	24.132(2)	24.051(2)
c [Å]	16.109(3)	16.289(5)	16.231(2)	16.222(2)	16.165(1)
M[46]	16.9	10.1	16.0	15.4	20.4
F[47]	42.0	23.1	37.1	35.9	48.3
R_{Bragg} [%]	2.72	1.50	1.40	2.40	1.27
χ^2	1.70	1.01	1.60	1.50	1.95

metry parameters, were allowed to refine freely. Fixed background points calculated with the WinPLOTR[44] interface were employed throughout the entire angular range. Table 5 collects the refined unit cell metrics, and Le Bail profile fittings (plus scanning electron microscopy images) for the microcrystalline powders **1**–**5** are provided as Figures S4–S8, respectively. The compound with Gd^{3+} (**7**) could only be isolated in small quantities, and, consequently, the signal-to-noise ratio for the PXRD pattern was very low. Nevertheless, indexation (not shown) confirmed the isomorphous nature with the remaining members of the series.

Photoluminescence Studies: Photoluminescence spectra were recorded at 12 K and at room temperature on a Fluorolog-3 Model FL3–2T with double excitation spectrometer and a single emission spectrometer (TRIAX 320) coupled to a R928 photomultiplier, by using the front face acquisition mode. The excitation source was a 450 W Xenon lamp. Emission was corrected for the spectral response of the monochromators and the detector by using typical correction spectra provided by the manufacturer, and the excitation spectra were corrected for the spectral distribution of the lamp intensity by using a photodiode reference detector. All spectra were acquired with 15 scans (averaging). The *Commission Internationale d'Éclairage*-CIE (x,y) emission colour coordinates were estimated for the 2° standard observer.

Supporting Information (see also the footnote on the first page of this article): Crystal morphology of single crystals of **1s**, **2s** and **6s** (optical photographs and SEM images), phase identification of microcrystalline powders of compounds **1**–**5** (whole powder-pattern decompositions with Le Bail extractions), FTIR vibrational spectra and thermograms for compounds **1**–**5** and **6s** and variable-temperature powder X-ray diffraction patterns for **6s** are presented.

Acknowledgments

We are grateful FSE and *Fundação para a Ciência e a Tecnologia* (Portugal) for their general financial support (PPCDT/QUI/58377/2004 and PTDC/QUI/65805/2006 supported by FEDER).

[1] S. R. Batten, R. Robson, *Angew. Chem. Int. Ed.* **1998**, *37*, 1461–1494; G. S. Papaefstathiou, L. R. MacGillivray, *Coord. Chem. Rev.* **2003**, *246*, 169–184; B. H. Ye, M. L. Tong, X. M. Chen, *Coord. Chem. Rev.* **2005**, *249*, 545–565; C. Janiak, *Dalton Trans.* **2003**, 2781–2804; N. R. Champness in *Making Crystals by Design – Methods, Techniques and Applications, 1st ed.* (Eds.: D. Braga, F. Grepioni), Wiley-VCH Verlag GmbH & Co. KGaA, Weinheim, **2007**, pp. 193–208; D. T. de Lill, C. L. Cahill in *Prog. Inorg. Chem. Vol. 55* (Ed.: K. D. Karlin), John Wiley & Sons, New Jersey, **2007**, pp. 143–203; B. Moulton, M. J. Zaworotko, *Chem. Rev.* **2001**, *101*, 1629–1658.

[2] M. D. Allendorf, R. J. T. Houk, L. Andruszkiewicz, A. A. Talin, J. Pikarsky, A. Choudhury, K. A. Gall, P. J. Hesketh, *J. Am. Chem. Soc.* **2008**, *130*, 14404–14405; C. A. Bauer, T. V. Timofeeva, T. B. Settersten, B. D. Patterson, V. H. Liu, B. A. Simmons, M. D. Allendorf, *J. Am. Chem. Soc.* **2007**, *129*, 7136–7144.

[3] S. Achmann, G. Hagen, J. Kita, I. M. Malkowsky, C. Kiener, R. Moos, *Sensors* **2009**, *9*, 1574–1589; X. D. Guo, G. S. Zhu, Z. Y. Li, F. X. Sun, Z. H. Yang, S. L. Qiu, *Chem. Commun.* **2006**, 3172–3174.

[4] F. Salles, D. I. Kolokolov, H. Jobic, G. Maurin, P. L. Llewellyn, T. Devic, C. Serre, G. Férey, *J. Phys. Chem. C* **2009**, *113*, 7802–7812; Y. C. Qiu, H. Deng, S. H. Yang, J. X. Mou, C. Daiguebonne, N. Kerbellec, O. Guillou, S. R. Batten, *Inorg. Chem.* **2009**, *48*, 3976–3981; E. Poirier, A. Dailly, *Energy Environ. Sci.* **2009**, *2*, 420–425; B. Mu, F. Li, K. S. Walton, *Chem. Commun.* **2009**, 2493–2495; J. A. Greathouse, T. L. Kinnibrugh, M. D. Allendorf, *Ind. Eng. Chem. Res.* **2009**, *48*, 3425–3431; Y. E. Cheon, M. P. Suh, *Chem. Commun.* **2009**, 2296–2298; R. Banerjee, H. Furukawa, D. Britt, C. Knobler, M. O'Keeffe, O. M. Yaghi, *J. Am. Chem. Soc.* **2009**, *131*, 3875–3877; D. Zhao, D. Q. Yuan, H. C. Zhou, *Energy Environ. Sci.* **2008**, *1*, 222–235; M. Dinca, A. Dailly, Y. Liu, C. M. Brown, D. A. Neumann, J. R. Long, *J. Am. Chem. Soc.* **2006**, *128*, 16876–16883; J. L. C. Rowsell, E. C. Spencer, J. Eckert, J. A. K. Howard, O. M. Yaghi, *Science* **2005**, *309*, 1350–1354; M. Dinca, J. R. Long, *J. Am. Chem. Soc.* **2005**, *127*, 9376–9377; H. Chun, D. N. Dybtsev, H. Kim, K. Kim, *Chem. Eur. J.* **2005**, *11*, 3521–3529.

[5] G. de Combarieu, M. Morcrette, F. Millange, N. Guillou, J. Cabana, C. P. Grey, I. Margiolaki, G. Férey, J. M. Tarascon, *Chem. Mater.* **2009**, *21*, 1602–1611.

[6] W. Ouellette, A. V. Prosvirin, K. Whitenack, K. R. Dunbar, J. Zubieta, *Angew. Chem. Int. Ed.* **2009**, *48*, 2140–2143; E. Q. Gao, Y. F. Yue, S. Q. Bai, Z. He, C. H. Yan, *J. Am. Chem. Soc.* **2004**, *126*, 1419–1429; V. Niel, A. L. Thompson, M. C. Munoz, A. Galet, A. S. E. Goeta, J. A. Real, *Angew. Chem. Int. Ed.* **2003**, *42*, 3760–3763; B. Q. Ma, S. Gao, G. Su, G. X. Xu, *Angew. Chem. Int. Ed.* **2001**, *40*, 434–437; Y. C. Liang, R. Cao, W. P. Su, M. C. Hong, W. J. Zhang, *Angew. Chem. Int. Ed.* **2000**, *39*, 3304–3307; D. Hagrman, R. P. Hammond, R. Haushalter, J. Zubieta, *Chem. Mater.* **1998**, *10*, 2091–2100.

[7] L. L. Zheng, H. X. Li, J. D. Leng, J. Wang, M. L. Tong, *Eur. J. Inorg. Chem.* **2008**, 213–217; K. J. Wei, J. Ni, M. Gao, Y. Z. Liu, Q. L. Liu, *Eur. J. Inorg. Chem.* **2007**, 3868–3880; X. L. Wang, C. Qin, E. B. Wang, Z. M. Su, Y. G. Li, L. Xu, *Angew. Chem. Int. Ed.* **2006**, *45*, 7411–7414; Q. Y. Liu, Y. L. Wang, L. Xu, *Eur. J. Inorg. Chem.* **2006**, 4843–4851; Y. Z. Zheng, M. L. Tong, X. M. Chen, *Eur. J. Inorg. Chem.* **2005**, 4109–4117; Q. Y. Liu, L. Xu, *Eur. J. Inorg. Chem.* **2005**, 3458–3466; J. Zhang, S. Gao, C. M. Che, *Eur. J. Inorg. Chem.* **2004**, 956–959.

[8] A. Simperler, M. D. Foster, O. D. Friedrichs, R. G. Bell, F. A. A. Paz, J. Klinowski, *Acta Crystallogr., Sect. B* **2005**, *61*, 263–279; C. Mellot-Draznieks, S. Girard, G. Férey, J. C. Schon, Z. Cancarevic, M. Jansen, *Chem. Eur. J.* **2002**, *8*, 4102–4113.

[9] G. Férey, C. Mellot-Draznieks, C. Serre, F. Millange, *Acc. Chem. Res.* **2005**, *38*, 217–225.

[10] F. A. A. Paz, J. Klinowski, *18th International Conference on Physical Organic Chemistry (ICPOC-18)*, Int Union Pure Ap-

plied Chemistry, Warsaw, Poland, **2006**, pp. 1097–1110; F. A. A. Paz, J. Rocha, J. Klinowski, T. Trindade, F. N. Shi, L. Mafra, *Prog. Solid State Chem.* **2005**, *33*, 113–125.

[11] F. N. Shi, L. Cunha-Silva, T. Trindade, F. A. A. Paz, J. Rocha, *Cryst. Growth Des.* **2009**, *9*, 2098–2109; P. C. R. Soares-Santos, L. Cunha-Silva, F. A. A. Paz, R. A. S. Ferreira, J. Rocha, T. Trindade, L. D. Carlos, H. I. S. Nogueira, *Cryst. Growth Des.* **2008**, *8*, 2505–2516; M. O. Rodrigues, N. B. da Costa, C. A. de Simone, A. A. S. Araujo, A. M. Brito-Silva, F. A. A. Paz, M. E. de Mesquita, S. A. Junior, R. O. Freire, *J. Phys. Chem. B* **2008**, *112*, 4204–4212; P. I. Girginova, F. A. A. Paz, P. C. R. Soares-Santos, R. A. S. Ferreira, L. D. Carlos, V. S. Amaral, J. Klinowski, H. I. S. Nogueira, T. Trindade, *Eur. J. Inorg. Chem.* **2007**, 4238–4246; P. C. R. Soares-Santos, F. A. A. Paz, R. A. S. Ferreira, J. Klinowski, L. D. Carlos, T. Trindade, H. I. S. Nogueira, *Polyhedron* **2006**, *25*, 2471–2482.

[12] L. Cunha-Silva, S. Lima, D. Ananias, P. Silva, L. Mafra, L. D. Carlos, M. Pillinger, A. A. Valente, F. A. A. Paz, J. Rocha, *J. Mater. Chem.* **2009**, *19*, 2618–2632; F. N. Shi, T. Trindade, J. Rocha, F. A. A. Paz, *Cryst. Growth Des.* **2008**, *8*, 3917–3920; L. Cunha-Silva, L. Mafra, D. Ananias, L. D. Carlos, J. Rocha, F. A. A. Paz, *Chem. Mater.* **2007**, *19*, 3527–3538.

[13] F. N. Shi, L. Cunha-Silva, R. A. S. Ferreira, L. Mafra, T. Trindade, L. D. Carlos, F. A. A. Paz, J. Rocha, *J. Am. Chem. Soc.* **2008**, *130*, 150–167.

[14] E. Chelebaeva, J. Larionova, Y. Guari, R. A. S. Ferreira, L. D. Carlos, F. A. A. Paz, A. Trifonov, C. Guerin, *Inorg. Chem.* **2008**, *47*, 775–777.

[15] G. Li, Y. T. Fan, T. J. Zhang, T. Z. Ge, H. W. Hou, *J. Coord. Chem.* **2008**, *61*, 540–549; H. Chen, Z. G. Sun, D. P. Dong, L. Meng, X. F. Zheng, Y. Y. Zhu, Y. Zhao, J. Zhang, *J. Coord. Chem.* **2008**, *61*, 1316–1324; Z. C. Zhang, S. Gao, L. M. Zheng, *Dalton Trans.* **2007**, 4681–4684; J. F. Xiang, M. Li, S. M. Wu, L. J. Yuan, J. T. Sun, *J. Coord. Chem.* **2007**, *60*, 1867–1875; D. K. Cao, Y. Z. Li, L. M. Zheng, *Inorg. Chem.* **2007**, *46*, 7571–7578.

[16] F. Y. Liu, L. Roces, R. A. S. Ferreira, S. Garcia-Granda, J. R. Garcia, L. D. Carlos, J. Rocha, *J. Mater. Chem.* **2007**, *17*, 3696–3701.

[17] B. Liu, B. L. Li, Y. Z. Li, Y. Chen, S. S. Bao, L. M. Zheng, *Inorg. Chem.* **2007**, *46*, 8524–8532.

[18] L. Van Meervelt, P. Martello, J. P. Silvestre, R. Rochdaoui, M. R. Lee, N. Q. Dao, C. Gorller-Walrand, *Z. Kristall.* **2002**, *217*, 27–34; K. L. Nash, R. D. Rogers, J. Ferraro, J. Zhang, *Inorg. Chim. Acta* **1998**, *269*, 211–223.

[19] L. Mafra, F. A. A. Paz, F. N. Shi, R. A. S. Ferreira, L. D. Carlos, T. Trindade, C. Fernandez, J. Klinowski, J. Rocha, *Eur. J. Inorg. Chem.* **2006**, 4741–4751.

[20] G. C. Aleksandrov, V. S. Sergienko, E. G. Afonin, *Crystallography. Rep.* **2001**, *46*, 46–50.

[21] S. Boudin, A. Guesdon, A. Leclaire, M. M. Borel, *Int. J. Inorg. Mater.* **2000**, *2*, 561–579.

[22] L. Carlucci, G. Ciani, D. M. Proserpio, *Coord. Chem. Rev.* **2003**, *246*, 247–289; L. Carlucci, G. Ciani, D. M. Proserpio, *CrystEngComm* **2003**, *5*, 269–279; I. A. Baburin, V. A. Blatov, L. Carlucci, G. Ciani, D. M. Proserpio, *J. Solid State Chem.* **2005**, *178*, 2452–2474; V. A. Blatov, L. Carlucci, G. Ciani, D. M. Proserpio, *CrystEngComm* **2004**, *6*, 377–395; O. Delgado-Friedrichs, M. D. Foster, M. O'Keeffe, D. M. Proserpio, M. M. J. Treacy, O. M. Yaghi, *J. Solid State Chem.* **2005**, *178*, 2533–2554.

[23] V. A. Blatov, A. P. Shevchenko, *TOPOS – Version 4.0* Professional (beta evaluation), Samara State University, Samara, Russia. **2006**; V. A. Blatov, A. P. Shevchenko, V. N. Serezhkin, *J. Appl. Crystallogr.* **2000**, *33*, 1193.

[24] *RCSR* (Reticular Chemistry Structure Resource), website: http://rcsr.anu.edu.au/.

[25] *EPINET*, Wwbsite: http://epinet.anu.edu.au.

[26] G. Socrates, *Infrared Characteristic Group Frequencies – Tables and Charts, 2nd ed.*, John Wiley & Sons Ltd., Baffins Lane, Chichester, **1994**.

[27] E. G. Afonin, *Russ. J. Gen. Chem.* **2001**, *71*, 75–78; E. G. Afonin, T. A. Matkovskaya, N. I. Pechurova, *Zh. Obshch. Khim.* **1988**, *58*, 1512–1516; E. G. Afonin, N. I. Pechurova, *Izv. Vyssh. Uchebn. Zaved., Khim. Khim. Tekhnol.* **1989**, *32*, 16–19; E. G. Afonin, N. I. Pechurova, *Zh. Obshch. Khim.* **1989**, *59*, 317–321.

[28] M. Anpo, I. Tanahashi, Y. Kubokawa, *J. Phys. Chem.* **1980**, *84*, 3440–3443; A. M. Gritscov, V. A. Shvets, V. B. Kazansky, *Chem. Phys. Lett.* **1975**, *35*, 511–512.

[29] E. Chelebaeva, J. Larionova, Y. Guari, R. A. S. Ferreira, L. D. Carlos, F. A. A. Paz, A. Trifonov, C. Guerin, *Inorg. Chem.* **2009**, DOI: 10.1021/ic900378d.

[30] T. Kottke, D. Stalke, *J. Appl. Cryst.* **1993**, *26*, 615–619.

[31] APEX2, *Data Collection Software Version 2.1-RC13*, Bruker AXS, Delft, The Netherlands, **2006**.

[32] Cryopad, *Remote monitoring and control, Version 1.451*, Oxford Cryosystems, Oxford, United Kingdom, **2006**.

[33] *SAINT+*, *Data Integration Engine v. 7.23a* © **1997–2005**, *Bruker AXS, Madison, Wisconsin, USA*.

[34] G. M. Sheldrick, *SADABS v.2.01, Bruker/Siemens Area Detector Absorption Correction Program* **1998**, Bruker AXS, Madison, Wisconsin, USA.

[35] G. M. Sheldrick, *SHELXS-97, Program for Crystal Structure Solution*, University of Göttingen **1997**.

[36] G. M. Sheldrick, *SHELXL-97, Program for Crystal Structure Refinement*, University of Göttingen **1997**.

[37] A. L. Spek, *J. Appl. Crystallogr.* **2003**, *36*, 7–13; A. L. Spek, *PLATON – A Multipurpose Crystallographic Tool*, Utrecht University, Utrecht, The Netherlands, **2007**.

[38] *SHELXL-97 Manual*, Bruker AXS, Inc., USA, **1997**.

[39] S. Parsons, *Acta Crystallogr., Sect. D* **2003**, *59*, 1995–2003.

[40] P. W. Betteridge, J. R. Carruthers, R. I. Cooper, K. Prout, D. J. Watkin, *J. Appl. Crystallogr.* **2003**, *36*, 1487.

[41] P. van der Sluis, A. L. Spek, *Acta Crystallogr., Sect. A* **1990**, *46*, 194–201.

[42] A. Boultif, D. Louer, *J. Appl. Crystallogr.* **2004**, *37*, 724–731.

[43] J. Rodriguez-Carvajal, *FULLPROF – A Program for Rietveld Refinement and Pattern Matching Analysis*, Abstract of the Satellite Meeting on Powder Diffraction of the XV Congress of the IUCR, Toulouse, France, **1990**, p.127.

[44] T. Roisnel, J. Rodriguez-Carvajal, *WinPLOTR [July 2006] – A Windows Tool for Powder Diffraction Pattern Analysis*, Materials Science Forum, Proceedings of the Seventh European Powder Diffraction Conference (EPDIC 7) (Ed.: R. Delhez and E. J. Mittenmeijer), **2000**, p.118–123.

[45] G. Caglioti, A. Paoletti, F. P. Ricci, *Nucl. Instr.* **1958**, *3*, 223–228.

[46] A. Boultif, D. Louer, *J. Appl. Crystallogr.* **1991**, *24*, 987–993.

[47] D. Louer in *Automatic Indexing: Procedures and Applications, Accuracy in Powder Diffraction II*, Gaithersburg, MD, USA, **1992**, pp. 92–104.

Received: June 19, 2009
Published Online: October 5, 2009

